

This represents a post-print of a peer-reviewed manuscript that has been accepted for publication in  
*Geochemistry, Geophysics, Geosystems* (acceptance date 31/08/2021).

1   **This manuscript has now been accepted for publication in**  
2   ***Geochemistry, Geophysics, Geosystems*. The published**  
3   **version of the manuscript can be found here:**

4   **<https://doi.org/10.1029/2021GC009932>**

5

6   **Please cite this manuscript as:**

7           Gleeson, M., Soderman, C., Matthews, S., Cottaar, S., & Gibson,  
8       S. (2021). Geochemical constraints on the structure of the Earth's deep mantle  
9       and the origin of the LLSVPs. *Geochemistry, Geophysics, Geosystems*, 22,  
10      e2021GC009932. <https://doi.org/10.1029/2021GC009932>

# 11    **Geochemical constraints on the structure of the Earth's deep** 12    **mantle and the origin of the LLSVPs**

13  
14    Matthew Gleeson<sup>1</sup>, Caroline Soderman<sup>2</sup>, Simon Matthews<sup>3</sup>, Sanne Cottaar<sup>2</sup>, Sally Gibson<sup>2</sup>

15    <sup>1</sup>School of Earth and Environmental Sciences, Cardiff University, Main Building, Park Place, CF10 3AT,  
16    UK.

17    <sup>2</sup>Department of Earth Sciences, University of Cambridge, Downing Street, Cambridge, CB2 3EQ, UK.

18    <sup>3</sup>Institute of Earth Sciences, University of Iceland, Sturlugata 7, 102 Reykjavik, Iceland.

## 19    **KEY POINTS**

---

- 20    1. Compositional variability in erupted basalts and olivine crystals reveals the distribution of  
21        recycled material in the Galápagos plume.  
22    2. The eastern Pacific LLSVP does not represent piles of subducted oceanic crust.  
23    3. Geochemical and geophysical data indicate the presence of recycled crustal material near  
24        the eastern margin of the Pacific LLSVP.

## 25    **ABSTRACT**

---

26    Geophysical analysis of the Earth's lower mantle has revealed the presence of two superstructures  
27    characterized by low shear wave velocities on the core-mantle boundary. These Large Low Shear  
28    Velocity Provinces (LLSVPs) play a crucial role in the dynamics of the lower mantle and act as the  
29    source region for deep-seated mantle plumes. However, their origin, and the characteristics of the  
30    surrounding deep mantle, remain enigmatic. Mantle plumes located above the margins of the  
31    LLSVPs display evidence for the presence of this deep-seated, thermally and/or chemically  
32    heterogeneous mantle material ascending into the melting region. As a result, analysis of the spatial  
33    geochemical heterogeneity in OIBs provides constraints on the structure of the Earth's lower mantle  
34    and the origin of the LLSVPs. In this study, we focus on the Galápagos Archipelago in the eastern  
35    Pacific, where bilateral asymmetry in the radiogenic isotopic composition of erupted basalts has

36 been linked to the presence of LLSVP material in the underlying plume. We show, using spatial  
37 variations in the major element contents of high-MgO basalts, that the isotopically enriched south-  
38 western region of the Galápagos mantle – assigned to melting of LLSVP material – displays no  
39 evidence for lithological heterogeneity in the mantle source. As such, it is unlikely that the Pacific  
40 LLSVP represents a pile of subducted oceanic crust. Clear evidence for a lithologically heterogeneous  
41 mantle source is, however, found in the north-central Galápagos, indicating that a recycled crustal  
42 component is present near the eastern margin of the Pacific LLSVP, consistent with seismic  
43 observations.

## 44 1 INTRODUCTION

---

45 Volcanic archipelagos such as the Galápagos, Hawai'i and Samoa represent the surface expression of  
46 deep-seated mantle plumes that likely originate near the core-mantle boundary (Morgan, 1971;  
47 Wilson, 1973). Such regions of ocean island volcanism provide an important window into the  
48 composition and structure of the Earth's lower mantle, which plays a critical role in the  
49 geodynamical and thermochemical evolution of the planet. For example, unradiogenic He (and Ne)  
50 isotope systematics (that is,  ${}^3\text{He}/{}^4\text{He} > 8 R/R_A$ ; where  $R/R_A$  indicates the measured ratio of  ${}^3\text{He}/{}^4\text{He}$   
51 relative to the  ${}^3\text{He}/{}^4\text{He}$  ratio of air) in ocean island basalts (OIBs) indicates that an undegassed,  
52 primordial component is likely preserved in the lower mantle over >4 billion years despite vigorous  
53 mantle convection (Farley et al., 1992; Jackson et al., 2010; Kurz and Geist, 1999; Stuart et al., 2003).  
54 In addition, the radiogenic isotope variability of OIBs provides evidence for recycling of lithospheric  
55 material into the deep mantle, resulting in the presence of several isotopically distinct mantle  
56 reservoirs (e.g. EM-1, EM-2, HIMU; Chauvel et al., 1992; Hofmann, 1997; Stracke et al., 2005; White  
57 and Hofmann, 1982; Willbold and Stracke, 2006). However, to fully understand the long-term  
58 evolution of the Earth's lower mantle, it is necessary to relate the chemical heterogeneities  
59 observed in OIBs to the detailed picture of the Earth's lower mantle that has been developed  
60 through various geophysical techniques.

61 Seismic tomography images of the Earth's lower mantle reveal that it is far from homogeneous.

62 Most notably, seismic models highlight the presence of two 'superstructures' on the core mantle

63 boundary that are characterized by lower shear wave velocities than the surrounding mantle

64 (Cottaar and Lekic, 2016; Dziewonski and Woodhouse, 1987; Garnero et al., 2016; Ritsema et al.,

65 2011) and are argued to have higher densities than surroundings (Lau et al., 2017; Moulik and

66 Ekström, 2016) at least at their base (Davaille and Romanowicz, 2020; Richards et al., 2021). These

67 superstructures, known as Large Low Shear Velocity Provinces (LLSVPs), are located beneath Africa

68 and the Pacific and play a critical role in mantle dynamics, the rise of mantle plumes (Heyn et al.,

69 2020), and the configuration of True Polar Wander events (Steinberger et al., 2017). Despite their

70 importance, however, the origin of the LLSVPs remain enigmatic, with their presence having

71 previously been assigned to piles of subducted oceanic crust (Brandenburg and van Keken, 2007;

72 Niu, 2018) or primordial material that has undergone differentiation early in Earth's history (such as

73 magma ocean cumulates; Deschamps et al., 2012; Labrosse et al., 2007; Peters et al., 2018).

74 Global seismic tomography models reveal that many mantle plumes are rooted within, or at the

75 margins of the LLSVPs, indicating that these regions represent 'plume nurseries' (Fig. 1; Doubrovine

76 et al., 2016; French and Romanowicz, 2015; Jackson et al., 2018). Furthermore, several mantle

77 plumes worldwide display bilateral asymmetry; where isotopically enriched signals are assigned to

78 melting of upwelling LLSVP material, and isotopically depleted compositions are related to melting

79 of the surrounding peridotitic mantle (Harpp et al., 2014b; Harpp and Weis, 2020; Hoernle et al.,

80 2015; Huang et al., 2011; Weis et al., 2011; Zhou et al., 2020). Therefore, a critical analysis of the

81 compositional variability displayed by one such mantle plume, considering all available isotopic,

82 trace element and major element data, has the potential to reveal new insights into the origin of the

83 LLSVPs, with implications for the evolution of the solid Earth over billion-year timescales. Specifically,

84 correlation of the isotopic and lithological heterogeneity (the latter inferred by major elements in

85 basalts and minor elements in olivine) observed in LLSVP-rooted plumes will allow the distribution of

86 recycled components in the lower mantle to be investigated and thus determine whether LLSVPs  
87 truly represent piles of subducted oceanic crust.

88 Here, we choose to focus on the Galápagos Archipelago, which is located above the eastern margin  
89 of the Pacific LLSVP and displays bilateral asymmetry in the trace element and radiogenic isotope  
90 composition of the erupted basalts (Harpp et al., 2014b; Harpp and Weis, 2020). We present new  
91 olivine data from the central Galápagos that, alongside published olivine and whole-rock data from  
92 across the archipelago, allows us to determine the spatial variability in the lithological structure of  
93 the underlying mantle plume. In doing so, we identify where recycled crustal components are  
94 directly involved in the genesis of Galápagos magmas (Herzberg, 2011; Rosenthal et al., 2015;  
95 Sobolev et al., 2005; Yaxley and Green, 1998). Finally, we discuss the implications of our findings for  
96 the structure of the lower mantle beneath the Pacific and the origin of the Pacific LLSVP.

97 **2 GEOLOGICAL BACKGROUND**

---

98 The Galápagos Archipelago is located ~1000 km off the western coast of Ecuador in the eastern  
99 equatorial Pacific and represents one of the most volcanically active regions in the world. Volcanism  
100 in the Galápagos is driven by melting in an upwelling mantle plume that has a mantle potential  
101 temperature ( $T_p$ ) >30 – 150 °C above that of the ambient mantle (Gibson et al., 2015). Seismic  
102 tomography provides evidence that the Galápagos mantle plume originates below the mantle  
103 transition zone, likely at the core-mantle boundary near the eastern margin of the Pacific LLSVP  
104 (Hooft et al., 2003; Nolet et al., 2019).

105 The Galápagos Archipelago lies on the eastward-moving Nazca tectonic plate (plate velocity of ~50  
106 km/Myr; Argus et al., 2011), about 150 – 200 km south of the Galápagos Spreading Centre, a plume-  
107 influenced segment of the global mid-ocean ridge system. Seismic tomography indicates that the  
108 Galápagos mantle plume is centered beneath the south-western Archipelago at ~200 km depth, but  
109 is deflected to the north-east at ~100 – 80 km depth owing to the presence of the nearby spreading

110 centre (Villagómez et al., 2014). The Galápagos Spreading Centre itself clearly shows the influence of  
111 the nearby mantle plume in the geochemical composition of the erupted basalts and the crustal  
112 thickness of the ridge (Canales et al., 2002; Christie et al., 2005; Cushman et al., 2004; Detrick et al.,  
113 2002; Gibson and Richards, 2018; Gleeson et al., 2020; Gleeson and Gibson (2021); Ingle et al., 2010;  
114 Schilling et al., 1982; Sinton et al., 2003).

115 Owing to the west-to-east motion of the Nazca tectonic plate, Galápagos volcanoes follow a general  
116 west-to-east age progression, with the youngest volcanic activity in the west and the oldest lavas  
117 observed on the eastern islands of San Cristobal and Espanola (Bailey, 1976; Geist et al., 1986;  
118 Naumann and Geist, 2000). However, volcanic activity in the central and eastern Galápagos persists  
119 into the Holocene, with historical eruptions observed on the central island of Santiago (Global  
120 Volcanism Program, 2013) and lavas as young as ~9 ka found on the eastern-most island of San  
121 Cristobal (Mahr et al., 2016). Nevertheless, some of the basalts from the eastern-most Galápagos  
122 may have erupted when the islands were located several 10s of km west of their current location.  
123 Yet, owing to the size of the Galápagos Archipelago (>400 km from west to east), and the dominance  
124 of more recent volcanic activity on the central and western Galápagos volcanoes, the composition of  
125 basalts erupted across the Galápagos Archipelago can be used to evaluate the spatial heterogeneity  
126 of the underlying mantle plume.

## 127 2.1 ISOTOPIC HETEROGENEITY OF THE GALÁPAGOS ARCHIPELAGO

128 Since the 1980s, analysis of radiogenic isotope ratios has dominated understanding of source  
129 heterogeneity in the Galápagos mantle plume (Geist et al., 1988; Harpp and Weis, 2020; Harpp and  
130 White, 2001; Hoernle et al., 2000; White et al., 1993). Specifically, spatial variability in the Pb, Nd, Hf  
131 and Sr isotope composition of the Galápagos basalts has traditionally been interpreted to represent  
132 the contribution of melts from at least 4 isotopically distinct end-members (Blichert-Toft and White,  
133 2001; Harpp and White, 2001). These end-members, known as PLUME, FLO, WD (Wolf-Darwin), and

134 DGM (Depleted Galápagos Mantle), are most strongly expressed in spatially defined regions of the  
135 Galápagos Archipelago and associated ridges (Harpp and White, 2001; Hoernle et al., 2000).  
  
136 The PLUME end-member is dominant in basalts from the westernmost island of Fernandina, and is  
137 characterized by moderately radiogenic Sr and Pb isotope signatures, similar to the common plume  
138 component referred to as 'FOZO' or 'C' (Hanan and Graham, 1996; Harpp and White, 2001). Notably,  
139 the Fernandina basalts have unradiogenic He and Ne isotope signatures (e.g.  ${}^3\text{He}/{}^4\text{He}$  up to 30 R/R<sub>A</sub>;  
140 Kurz and Geist, 1999), which indicates the presence of an undegassed primordial reservoir in the  
141 Galápagos plume.  
  
142 To the south of Fernandina, basalts trend towards more radiogenic Sr and Pb isotope signatures,  
143 which reach a maximum on the southern island of Floreana (Harpp et al., 2014a; Harpp and White,  
144 2001; Kurz and Geist, 1999). The extreme radiogenic isotope composition of Floreana (that is,  
145 elevated  ${}^{206}\text{Pb}/{}^{204}\text{Pb}$  and  ${}^{187}\text{Os}/{}^{188}\text{Os}$  ratios) is used to define the FLO mantle end-member, which  
146 displays similar  ${}^{206}\text{Pb}/{}^{204}\text{Pb}$  signatures to the global HIMU mantle (Gibson et al., 2016; Harpp et al.,  
147 2014a). As a result, the FLO mantle is hypothesized to represent recycled Archean oceanic crust  
148 (Gibson et al., 2016; Harpp et al., 2014a), although the absence of evidence for a pyroxene-rich  
149 component in the mantle source of the Floreana lavas casts doubt on the recycled crustal origin  
150 (Gleeson et al., 2021; Vidito et al., 2013).  
  
151 Basalts in the eastern Galápagos (i.e. Genovesa, San Cristobal and eastern Santiago) are dominated  
152 by melts of the DGM (Gibson et al., 2012; Harpp and White, 2001). However, whether the DGM  
153 component is entrained upper mantle, or derives from the lower mantle, is an ongoing area of  
154 debate (Blichert-Toft and White, 2001; Gibson et al., 2012; Harpp and Weis, 2020; Hoernle et al.,  
155 2000). Finally, the WD isotopic end-member is restricted to a small number of seamounts and minor  
156 islands in the northernmost Galápagos and appears to have little to no influence on the composition  
157 of basalts elsewhere in the Galápagos (Harpp and White, 2001). The origin of this localized  
158 component is unknown and is not addressed in this study.

159 The complex relationship between the different mantle end-members identified in the Galápagos  
160 mantle plume has made correlation of these signatures to the structure of the underlying deep  
161 mantle very challenging. It is possible, however, to simplify the spatial heterogeneity observed in the  
162 radiogenic isotope composition of the Galápagos basalts and instead describe their variability in  
163 terms of overall isotopic enrichment (Harpp and Weis, 2020). The most enriched isotopic signatures  
164 (here used to describe radiogenic Pb and Sr and unradiogenic Nd isotope compositions) are  
165 observed in the western and southern Galápagos, whereas isotopically depleted compositions  
166 dominate in the north-eastern Galápagos (apart from Pinta, whose anomalously enriched  
167 composition is likely related to plume-ridge interactions in the Galápagos; Fig. 2a).

168 Critically, this isotopic variability mirrors the structure of the deep mantle at the base of the  
169 Galápagos mantle plume, with LLSVP material to the south-west and ‘normal’ lower mantle to the  
170 north-east (Fig. 1 & 2; Cottaar and Lekic, 2016; Garnero et al., 2016; Ritsema et al., 2011). As a result,  
171 the enriched isotopic signatures of the south-western Galápagos have been assigned to melting of  
172 LLSVP material ascending as part of the Galápagos mantle plume, whereas the depleted nature of  
173 the north-eastern Galápagos basalts is hypothesized to result from melting of the surrounding  
174 peridotitic mantle (Harpp et al., 2014b; Harpp and Weis, 2020).

## 175 2.2 LITHOLOGICAL PROPERTIES OF THE GALÁPAGOS MANTLE PLUME

176 Our current understanding of the structure and composition of the Galápagos mantle plume is  
177 complicated by the unclear relationship between lithological and radiogenic isotopic heterogeneity  
178 (Gleeson et al., 2020; Gleeson and Gibson, 2019; Vidito et al., 2013). Lithological heterogeneity, that  
179 is, the presence of fusible, pyroxene-rich components in the underlying mantle, is believed to result  
180 from recycled crustal components in the mantle and their incorporation into upwelling mantle  
181 plumes (Gibson, 2002; Hauri, 1996; Lambart, 2017; Lambart et al., 2013; Mallik and Dasgupta, 2012;  
182 Rosenthal et al., 2015; Shorttle et al., 2014; Sobolev et al., 2007, 2005; Yaxley and Green, 1998). As  
183 such, identification of lithological heterogeneity in the mantle source region of basaltic lavas

184 provides evidence for the contribution of recycled crustal components to mantle plumes. Therefore,  
185 linking signatures of lithological heterogeneity to the isotopic heterogeneity of the Galápagos mantle  
186 plume might help to identify whether the LLSVPs truly represent piles of subducted oceanic crust.

187 Lithological heterogeneity in the mantle is commonly tracked through the minor element  
188 composition of olivine phenocrysts (Gurenko et al., 2013, 2009; Herzberg, 2011; Sobolev et al., 2007,  
189 2005). Specifically, high Ni but low Mn and Ca contents in primitive olivine phenocrysts are thought  
190 to be characteristic of a contribution from pyroxenite-derived melts, owing to the large differences  
191 in the bulk partition coefficient of these elements during melting of an olivine-rich (peridotite) and a  
192 pyroxene-rich (pyroxenite) lithology.

193 The composition of olivine crystals from the Galápagos Archipelago has previously been used to  
194 evaluate the lithological structure of the underlying plume, with initial interpretations suggesting  
195 that lithologically distinct components are present in both isotopically enriched and isotopically  
196 depleted regions of the Galápagos (Vidito et al., 2013). However, the presence of a pyroxenitic  
197 component in the mantle source region of the eastern Galápagos basalts contradicts their  
198 isotopically depleted nature and trace element systematics (e.g. Gibson et al., 2012). As a result, the  
199 anomalously high Ni and low Ca contents of the eastern Galápagos olivines were recently revisited,  
200 with numerical models of fractional crystallisation, magma recharge and diffusive re-equilibration  
201 demonstrating that these ‘pyroxenitic’ olivine compositions could be generated through crustal  
202 processing of basaltic lavas (Gleeson and Gibson, 2019).

203 Nevertheless, it remains possible that pyroxenitic source components contribute to basalts from  
204 other regions of the Galápagos. In fact, analysis of Fe-isotope ratios in basaltic lavas from plume-  
205 influenced regions of the Galápagos Spreading Centre (GSC) revealed that an enriched pyroxenitic  
206 component is present in the Galápagos mantle plume (Gleeson et al., 2020). However, it remains  
207 uncertain whether the enriched pyroxenite in the mantle source region of the GSC basalts is related  
208 to the isotopically enriched signatures assigned to melting of the LLSVP material contained within

209 the Galápagos mantle plume. To address this, we collect new olivine data from the central  
210 Galápagos, which is used alongside published olivine and whole-rock data from across the Galápagos  
211 Archipelago to evaluate the spatial variability in the lithological properties of the underlying mantle.

212 **3 METHODS**

---

213 We present high-precision analyses of the major and minor element composition of olivine crystals  
214 in geochemically enriched basalts from western Santiago in the central Galápagos. Previous work on  
215 the major element, trace element and isotopic composition of the Santiago basalts has led to the  
216 classification of four chemical groups: low-K tholeiites, high  $\epsilon_{\text{Nd}}$  transitional basalts, low  $\epsilon_{\text{Nd}}$   
217 transitional basalts, and mildly-alkaline basalts (Gibson et al., 2012). In general, the low-K tholeiites  
218 are found on the eastern side of the island, with enriched isotopic signatures found in mildly-alkaline  
219 basalts further west (Gibson et al., 2012). Our new data from well-characterised mildly alkaline and  
220 low  $\epsilon_{\text{Nd}}$  transitional basalts fills a crucial gap in the olivine data from the Galápagos, as olivine  
221 compositions from western and eastern Galápagos basalts (including eastern Santiago) have  
222 previously been characterized (Gleeson and Gibson, 2019; Vidito et al., 2013).

223 All data were collected using a Cameca SX100 electron microprobe in the Department of Earth  
224 Sciences, University of Cambridge. Analysis was carried out using a defocused (5  $\mu\text{m}$ ) spot and a 15  
225 kV accelerating voltage. Analysis of Si, Fe, and Mg was carried out using a 20 nA beam current. To  
226 increase the analytical precision on low concentration elements, a 100 nA beam current was used  
227 for analysis of Ni, Mn, Ca and Al. Mineral and metal standards were used to calibrate at the start of  
228 the analytical session and precision and accuracy were tracked through repeat analysis of a San  
229 Carlos Olivine secondary standard. Recovery for all elements is between 99 and 103%. The 2-sigma  
230 analytical precision of analysis is ~3% for Fe, better than 1.5% for Mg and Si, ~4% for Ni, ~15% for Ca,  
231 and ~8% for Mn (Supplementary Data).

232 **4 RESULTS**

---

233 Our new analyses reveal that olivines in mildly alkaline basalts from Isla Santiago (such as sample  
234 08DSG33) are relatively evolved, with forsterite (Fo) contents ranging from ~70 – 84, and contain  
235 moderately high Ni contents (~800 – 2900 ppm; Fig. 3). Olivines in mildly alkaline basalts also contain  
236 relatively low Mn contents (~1500 – 2500 ppm), and correspondingly high Fe/Mn ratios (72.8 ±5.2;  
237 Fig. 3). In contrast, the Fo contents of olivines from transitional basalt 07DSG61 are slightly more  
238 primitive than those observed in the mildly alkaline basalts (Fo ~81-85). Furthermore, the Ni content  
239 and Fe/Mn ratio of olivines in sample 07DSG61 are lower than those observed in the mildly alkaline  
240 basalts (~1200 – 2300 ppm and 71.1 ±5.1, respectively; Fig. 3).

241 **5 DISCUSSION**

---

242 **5.1 OLIVINE MINOR ELEMENT SYSTEMATICS**

243 Olivine minor elements provide a powerful method for investigating the lithological properties of the  
244 mantle (Gurenko et al., 2009; Herzberg et al., 2014; Sobolev et al., 2007), as long as the influence of  
245 crustal processes and the conditions of mantle melting are considered (Gleeson and Gibson, 2019;  
246 Matzen et al., 2013, 2017b). Olivine data from the eastern Galápagos (that is, San Cristobal,  
247 Genovesa and Espanola) indicate that the mantle source regions of these basalts are dominated by  
248 peridotite (Vidito et al., 2013; Fig. 3a,b). However, interpretation of olivine data from elsewhere in  
249 the Galápagos is not so simple (Gleeson and Gibson, 2019).

250 Taken at face value, the Ca content (and to a lesser extent the Ni content) of olivines in basalts from  
251 Floreana in the southern Galápagos, which originates from melting of LLSVP material with highly  
252 radiogenic Pb isotope signatures (Harpp and Weis, 2020), suggests that there is a notable  
253 contribution from melts from a pyroxenitic source component (Gleeson et al., 2021; Harpp et al.,  
254 2014a; Vidito et al., 2013). However, the low Ca contents and moderately high Ni contents observed  
255 in some of the Floreana olivines can instead be explained by chemical modification in a cumulate

256 mush (Gleeson et al., 2021). As such, there is no significant evidence in the olivine minor element  
257 systematics of the Floreana basalts to indicate that there is a substantial contribution of melts from  
258 a pyroxenitic source component (Fig. 3).

259 Olivine data from the western Galápagos (that is, the islands of Isabela, Roca Redonda, and  
260 Fernandina) display a range of compositions. Notably, it is clear that the Ni, Fe/Mn and Ca contents  
261 of olivines from Fernandina and Cerro Azul (on the southern margin of Isabela), which fall into the  
262 isotopically enriched south-western region of the archipelago, are consistent with the presence of a  
263 peridotite source (especially once the influence of crustal processes are taken into account; Gleeson  
264 and Gibson, 2019; Vidito et al., 2013). However, evidence for the contribution of melts from a  
265 pyroxenitic source component is found in the Fe/Mn ratio of olivines from Roca Redonda and  
266 Volcans Ecuador, Wolf and Darwin on Northern Isabela ( $\text{Fe}/\text{Mn} > 70$ ; Fig. 3 & 4; Vidito et al., 2013).  
267 Notably, the Ni contents of olivine from Roca Redonda and Volcan Ecuador are also higher than the  
268 olivine compositions predicted by the magma mixing models of Gleeson and Gibson (2019),  
269 supporting the interpretation that a pyroxenitic source contributes to the olivine composition of  
270 these Northern Isabela and Roca Redonda basalts. High Fe/Mn ratios ( $> 75$ ) are also found in olivines  
271 from Sierra Negra, but the evolved nature of the Sierra Negra basalts (often  $< 5$  wt% MgO) and  
272 olivines mean that we cannot rule out these signatures originating through crustal processing (cf.  
273 Trela et al., 2015).

274 In the central Galápagos, olivine data from mildly-alkaline basalts E-76 and 08GSD33 on western  
275 Santiago, reveal Ni and Fe/Mn contents that are too high to be explained by melting of a peridotitic  
276 source, even if the influence of crustal processes are considered (Gleeson and Gibson, 2019).  
277 Although care must be used when comparing the composition of magmatic olivines to the  
278 composition of their host basalt, as olivine crystals might not be directly related to their carrier melt  
279 (Wieser et al., 2019), it is notable that these basalts display the most enriched trace element and  
280 isotopic signatures of any basalt found on Santiago (Gibson et al., 2012). Conversely, olivine data

281 from isotopically depleted basalts on eastern Santiago are consistent with a dominant contribution  
282 of melts from a peridotitic source lithology (Gibson et al., 2016; Gleeson and Gibson, 2019).  
283 Transitional basalts from Santiago (such as 07DSG61) display intermediate olivine compositions at  
284 moderately high Ni and Fe/Mn contents, confirming that these basalts represent a mixture of  
285 pyroxenite and peridotite derived melts.

286 Olivine compositions from Santa Cruz in the central Galápagos fall into two groups, although the  
287 compositions measured within each sample are typically relatively uniform (Vidito et al., 2013). One  
288 group displays Fe/Mn contents between 60 and 72 (that is, consistent with a peridotitic source;  
289 Herzberg, 2011), whereas the other contains Fe/Mn ratios >70. The high Fe/Mn group also contains  
290 high Ni contents that cannot be easily explained by crustal processing of peridotite-derived basaltic  
291 magmas (Gleeson and Gibson, 2019). As such, the variability in the olivine composition of basalts  
292 from Santa Cruz likely results from changes in the proportion of pyroxenite-derived melt. The olivine  
293 compositional characteristics of Santa Cruz does not appear to define a geographic geochemical  
294 trend, unlike on Santiago (Gibson et al., 2012), with shorter length-scale variability in the  
295 composition of erupted basalts dominating.

296 Overall, the new and compiled olivine data indicates that a pyroxenitic, recycled component is  
297 present in the Galápagos mantle plume. However, this pyroxenitic component is not dominant in  
298 basalts of the isotopically enriched south-western region of the Galápagos. Instead, it is most  
299 prevalent in basalts from the north-central Galápagos, that is, mildly-enriched basalts from northern  
300 Isabela, Roca Redonda, western Santiago, and Santa Cruz (Fig. 4a). Importantly, our results indicate  
301 that geochemically enriched peridotite and pyroxenite components exist in the Galápagos mantle  
302 plume; as a result, there is no simple relationship between host-basalt enrichment and olivine Ni and  
303 Mn contents across the archipelago. Nevertheless, the proposed contribution of pyroxenitic melts to  
304 the north-central Galápagos basalts is supported by the isotopic similarity of these basalts (with

305 regards to Sr, Nd and Pb) to the pyroxenitic end-member previously identified in the mantle source  
306 region of the GSC basalts (Gleeson et al., 2020; Gleeson and Gibson, 2021; Fig. 5).

307 **5.2 MAJOR ELEMENT SYSTEMATICS OF THE GALÁPAGOS BASALTS**

308 Alongside olivine minor element compositions and Fe-isotope ratios of basaltic lavas, information  
309 about the lithological properties of the mantle source is contained in the major element systematics  
310 of high-MgO basalts (i.e., those that have not undergone significant fractionation of clinopyroxene  
311 or plagioclase; Dasgupta et al., 2010; Hauri, 1996; Lambart et al., 2016, 2013; Shorttle et al., 2014;  
312 Shorttle and MacLennan, 2011). Specifically, melts of a pyroxenitic source lithology often have lower  
313 CaO contents, and higher FeO<sub>t</sub> contents (where FeO<sub>t</sub> represents the total Fe content of the melt  
314 expressed as FeO), than melts of a peridotite (Herzberg, 2011; Hirose and Kushiro, 1993; Lambart et  
315 al., 2016, 2012).

316 To evaluate the spatial variability in the major element composition of primary mantle melts from  
317 the Galápagos, we compiled whole-rock major element data from across the archipelago and filtered  
318 the resulting dataset to exclude any samples with MgO contents <8 wt% (i.e., those that display  
319 substantial evidence for clinopyroxene and plagioclase fractionation; see Supplementary  
320 Information). Basalts in the filtered database contain a relatively narrow range of Mg# compositions  
321 (from ~55 to ~75 where Mg# = Mg/(Mg+Fe<sub>t</sub>) molar). However, variations in other major element  
322 parameters are observed.

323 Notably, the FeO<sub>t</sub> content of high-MgO basalts from the western, southern and eastern Galápagos  
324 are consistently <11 wt%, and typically less than 10.5 wt%. Melting experiments at pressures  
325 between 1.5 and 3 GPa on the KLB-1 peridotite (a commonly used experimental analogue for the  
326 upper mantle) provide mean FeO<sub>t</sub> contents of 8.88 wt%, and maximum FeO<sub>t</sub> contents of 10.05 wt%,  
327 broadly consistent with the compositions observed in the western, southern and eastern Galápagos  
328 (Fig. 2b; Fig. 4; Hirose and Kushiro, 1993; Takahashi et al., 1993). Furthermore, melting calculations  
329 performed in the KNCFMASTOCr system using THERMOCALC v3.4.7 reveal that melts produced by

330 the KLB-1 peridotite between 1.5 and 3 GPa, and at melt fractions less than 20% (see Supplementary  
331 Information), contain approximately  $9.77^{+1.09}_{-1.99}$  wt% FeO<sub>t</sub> (Holland et al., 2018; Holland and Powell,  
332 2011; Powell et al., 1998), almost perfectly overlapping with the FeO<sub>t</sub> content of the western,  
333 southern and eastern Galápagos basalts ( $9.74^{+0.94}_{-0.98}$  wt% FeO<sub>t</sub>; Fig. 4). Melts produced in hydrous  
334 melting regimes at significantly higher pressures (>3 GPa) are volumetrically minor, and therefore  
335 unlikely to influence the major element systematics of the Galápagos basalts and not considered  
336 here. In addition, the CaO contents of primitive basaltic magmas in the southern, eastern and  
337 western Galápagos are also consistent with the CaO content predicted from melting of a peridotite  
338 source (Hirose and Kushiro, 1993; Takahashi et al., 1993). As such, basalts in these regions of the  
339 Galápagos are likely dominated by melts of a peridotite source, with only a minor-to-moderate  
340 contribution from melts of a pyroxenitic component (<0 - 30 %), broadly consistent with the  
341 compositions observed in olivine crystals from these basalts (see above).

342 Some basalts in the north-central Galápagos, that is, Santa Cruz and western Santiago, the northern  
343 margin of Isabela (Volcan Ecuador) and Roca Redonda, display FeO<sub>t</sub> contents >11 wt%. In fact, on  
344 western Santiago and Roca Redonda, the whole-rock FeO<sub>t</sub> contents extend to >12.5 wt%, well  
345 outside the range of FeO<sub>t</sub> contents that can result from melting of a peridotite source lithology (Fig.  
346 4; Gibson et al., 2000; Hirose and Kushiro, 1993). Even if basalts from Roca Redonda with MgO  
347 contents >15 wt%, which may have assimilated high-FeO<sub>t</sub> olivine, are excluded the whole-rock FeO<sub>t</sub>  
348 contents of the remaining basalts are notably higher than those of the south-western and eastern  
349 Galápagos (~11 – 12 wt%; Supplementary Information). In addition, it is unlikely that a substantial  
350 increase in the depth of melting beneath the north-central Galápagos (relative to the western  
351 Galápagos) could explain this shift to higher FeO<sub>t</sub> contents, as the lithosphere is thickest and the  
352 mantle potential temperature is greatest beneath the south-western region of the archipelago  
353 where low FeO<sub>t</sub> values are observed (Gibson and Geist, 2010).

354 The high FeO<sub>t</sub> contents of the north-central Galápagos are consistent with the FeO<sub>t</sub> concentrations  
355 measured in experimental melts of pyroxenitic lithologies such as MIX-1g and M5-40 (Hirschmann et  
356 al., 2003; Kogiso et al., 2003; Lambart et al., 2013). Melting simulations in THERMOCALC v3.4.7 again  
357 support the experimental data, and demonstrate that melts of MIX-1g at pressures above 1.5 GPa,  
358 and melt fractions below 60%, contain  $11.54^{+2.22}_{-1.88}$  wt% FeO<sub>t</sub>, indicating a strong contribution of  
359 melts from a pyroxenitic source to the basalts of the north-central Galápagos ( $10.95^{+1.44}_{-1.13}$  wt% FeO<sub>t</sub>;  
360 Fig. 4). Notably, the regions of the northern and central Galápagos that display basalt FeO<sub>t</sub> contents  
361 >11 wt% all plot very close to the region where olivine minor element chemistry indicates the  
362 presence of a recycled pyroxenitic source component (Fig. 3 & 4).

363 In addition, a more detailed look at the central Galápagos (that is, Santiago, Santa Cruz, Santa Fe and  
364 Rabida), demonstrates that the major element variability observed across the Galápagos Archipelago  
365 is related to the degree of trace element and isotopic enrichment (Fig. 6 & 7). For example, high-  
366 MgO basalts with high FeO<sub>t</sub> and low CaO contents, which are inconsistent with the composition of  
367 melts produced by a peridotite source, are typically characterized by moderately radiogenic Pb and  
368 Sr isotope ratios and enriched trace element systematics (e.g. Nb/Y > 0.4; Gibson et al., 2012).  
369 Furthermore, comparison of experimental melt compositions to the observed major element  
370 systematics of the central Galápagos basalts has previously shown that the compositional variations  
371 across Isla Santiago are consistent with the presence of both pyroxenite and peridotite components  
372 in the mantle source, an observation that is consistent with the THERMOCALC v3.4.7 calculations  
373 presented here (Supplementary Information; Gleeson et al., 2020).

374 The high FeO<sub>t</sub> contents of the central Galápagos and Northern Isabela/Roca Redonda basalts are also  
375 expressed in their anomalously high Fe/Mn ratios (>65; Fig. 5b). However, unlike the FeO<sub>t</sub> and CaO  
376 contents of basalts from across the Galápagos Archipelago, there is a slight difference in the Fe/Mn  
377 ratio of basalts from the western Galápagos (Fernandina and Southern Isabela; ~60) and the eastern  
378 Galápagos (Espanola and San Cristobal; ~55). Variations in the Fe/Mn ratio of basaltic magmas have

379 traditionally been assigned to the presence of a fusible, pyroxenitic component (Herzberg, 2011) or a  
380 core component (Humayun et al., 2004) in the mantle source. Yet, the slight variation in the Fe/Mn  
381 ratio of the western and eastern Galápagos basalts could be explained by differences in the depth of  
382 melting (Matzen et al., 2017a), consistent with the greater lithospheric thickness in the western  
383 Galápagos compared to the eastern Galápagos (Gibson et al., 2012; Gibson and Geist, 2010).  
384 Nevertheless, the higher Fe/Mn ratio of the north-central Galápagos basalts requires a substantial  
385 contribution from melts of a pyroxenitic source, as these signatures cannot be generated by  
386 variations in the melting processes alone (Fig. 5b).

387 Overall, variations in the major element systematics of primitive basaltic lavas from across the  
388 Galápagos Archipelago indicate that a pyroxenitic component is present in the underlying mantle  
389 plume and is most strongly expressed in the composition of basalts from the north-central  
390 Galápagos basalts (northern Isabela, Roca Redonda, western Santiago and Santa Cruz). This  
391 hypothesis is supported by the similarity between the radiogenic isotope composition of the most  
392 enriched basalts from the north-central Galápagos (on Roca Redonda and western Santiago;  
393 Standish et al., 1998; Gibson et al. 2012) and the proposed isotopic composition of the pyroxenitic  
394 end-member in the mantle source region of the GSC basalts (Fig. 5; Gleeson et al., 2020; Gleeson  
395 and Gibson, 2021). As a result, the major element systematics of the primitive Galápagos basalts  
396 indicate that an isotopically enriched pyroxenitic source component contributes to both basalts from  
397 the north-central Galápagos, consistent with our interpretations based on the available olivine data  
398 shown above, and the GSC.

399 The spread of isotopic compositions observed in basalts from both the south-western and eastern  
400 Galápagos indicates that a small contribution of Sr, Pb and Nd-rich melts from this pyroxenitic  
401 component (i.e., <<25% pyroxenitic melt) might influence the radiogenic isotope ratios of basalts  
402 erupted across the entire archipelago (Fig. 8). There is, however, no evidence in the major element  
403 systematics of basalts from Fernandina, Southern Isabela and Floreana to indicate that there is a

404 large contribution of melts from this pyroxenitic component to the major element composition of  
405 basalts in the isotopically enriched south-western region of the archipelago (Fig. 4). Additionally, the  
406 major element systematics of the eastern Galápagos basalts provide no evidence to support  
407 previous interpretations of a depleted pyroxenitic component is dominant in the eastern Galápagos  
408 (Vidito et al., 2013).

### 409 5.3 VARIATIONS IN SOURCE PYROXENITE PROPORTIONS

410 The major element systematics of high-MgO basalts, and the minor element contents of their olivine  
411 cargo, reveal clear variations in the contribution of pyroxenitic melts to basalts erupted across the  
412 Galápagos Archipelago. However, it is important to consider whether the prevalence of pyroxenitic  
413 melt signatures in the north-central region of the Galápagos represents true spatial heterogeneity in  
414 the distribution of pyroxenitic components in the underlying Galápagos mantle plume, or if these  
415 signatures can instead be caused by variations in mantle potential temperature, melt extents, and  
416 melt extraction processes. Addressing this question is critical to understanding the distribution of  
417 lithologically distinct, recycled components in the Earth's lower mantle.

418 As pyroxenitic source components are typically more fusible than 'normal' mantle peridotite, the  
419 pyroxenite solidus will be crossed at higher pressures than the peridotite solidus during adiabatic  
420 decompression melting (Gibson et al., 2000; Kogiso et al., 2003; Lambart et al., 2016, 2013; Sobolev  
421 et al., 2007; Yaxley and Green, 1998). Therefore, melts of a pyroxenitic source dominate at low total  
422 melt fractions during melting of a two- or three-component mantle, with peridotite-derived melts  
423 becoming more dominant at shallower pressures (Lambart et al., 2016). As a result, the proportion  
424 of pyroxenite-derived melt contributing to the composition of basaltic lavas is influenced by  
425 variations in the mantle potential temperature and lithospheric thickness, as well as the proportion  
426 of pyroxenite in the source.

427 To address whether variations in melting parameters could explain the spatial variability in the  
428 contribution of pyroxenitic melts to the Galápagos Archipelago, we calculate the proportion of

429 pyroxenite-derived melt that results from melting of a two-component mantle under various  
430 conditions. Calculations were performed using the pymelt Python module (Matthews et al., 2020),  
431 and recent empirical parameterisations for the melting of a Iherzolitic peridotite and silica-  
432 undersaturated pyroxenite (KLB-1 and KG1, respectively; Matthews et al., 2021). We ran the  
433 calculations over a range of mantle potential temperatures ( $T_p = 1400 - 1460^\circ\text{C}$ ) and lithospheric  
434 thicknesses (46 – 60 km; ~1.5 – 1.85 GPa) appropriate to the Galápagos Archipelago (Gibson et al.,  
435 2015, 2012; Gibson and Geist, 2010; Herzberg and Asimow, 2008; Vidito et al., 2013), and consider  
436 how these conditions may influence the relative contribution of melts from a mixed peridotite-  
437 pyroxenite mantle source. For example, the pymelt models indicate that a mantle containing ~10%  
438 pyroxenite, melting at a  $T_p$  of 1400 °C under 60 km thick lithosphere produces magmas with a  
439 pyroxenite melt proportion of ~70%. Melting of the same mantle with a  $T_p$  of 1460°C and a  
440 lithospheric thickness of ~46 km gives a pyroxenitic melt proportion of only ~30%.

441 To determine whether variations in the conditions of mantle melting across the Galápagos  
442 Archipelago can cause the observed differences in the relative contribution of pyroxenitic melts to  
443 the Galápagos basalts, we compare the results of our melting calculations to first-order estimates of  
444 the proportion of pyroxenitic melt that contributes to each region of the Galápagos. These estimates  
445 are derived from the mean  $\text{FeO}_t$  content of the Galápagos basalts, an assumed peridotite melt  $\text{FeO}_t$   
446 content of 8.8 – 9.77 wt% and a pyroxenite melt  $\text{FeO}_t$  content of 12.8 wt% (representing the mean  
447  $\text{FeO}_t$  content of the experimental and thermodynamic KLB-1 melts and the highest  $\text{FeO}_t$  content  
448 observed in any of the Galápagos basalts, respectively). Results indicate that basalts from the  
449 western and eastern Galápagos contain, on average, a 0 – 24% contribution of melts from a  
450 pyroxenitic source (mean  $\text{FeO}_t$  of 9.75 wt%), whereas basalts from western Santiago contain 57 –  
451 80% pyroxenitic melts ( $\text{FeO}_t$  contents between 11.5 and 12 wt%). This variation is similar in  
452 magnitude to the maximum difference in the proportion of pyroxenitic melt that can be caused by  
453 variations in the melting conditions of a homogeneous mantle source beneath the Galápagos  
454 Archipelago (~30 – 70%; Fig. 9).

455 Regions of the Galápagos Archipelago that are dominated by melts of peridotitic source lithologies,  
456 however, do not only occur in regions where the lithosphere is thinnest or where the mantle  
457 potential temperature is highest. For example, Isla Fernandina and Volcan Cerro Azul, on southern  
458 Isabela, display no evidence for the contribution of pyroxenitic melts, despite the fact that seismic  
459 data indicates the lithosphere is thickest in this region of the archipelago (Fig. 2c; Gibson and Geist,  
460 2010; Rychert et al., 2014). As such, it is unlikely that variations in the contribution of pyroxenitic  
461 melts to basalts erupted across the Galápagos Archipelago results purely from variations in the  
462 melting conditions. Instead, we suggest that the difference in the proportion of pyroxenitic melt  
463 contributing to basalts from the south-western, north-central and north-eastern regions of the  
464 Galápagos Archipelago must result from variations in the proportion of pyroxenite present in the  
465 mantle source. We note that the first-order estimates for the proportion of pyroxenitic melt  
466 contributing to each region of the Galápagos presented above can be recreated when the mantle  
467 source region of the western, southern and eastern Galápagos contains <5 % pyroxenite, but the  
468 mantle source region of the north-central Galápagos basalts contains >20% pyroxenite (Fig. 9).  
  
469 In addition, the presence of at least three distinct components in the Galápagos mantle plume are  
470 required by the radiogenic isotope variability of the Galápagos basalts. Specifically, we note that the  
471  $^{87}\text{Sr}/^{86}\text{Sr}$  isotope signature of the north-central Galápagos basalts (pyroxenite source) are lower than  
472 that observed in basalts from the south-western Galápagos (peridotite source; Fig. 5). This indicates  
473 that basalts in the south-western archipelago cannot be a mixture of melts derived from an enriched  
474 pyroxenite and a depleted peridotite, otherwise they would display a less enriched radiogenic  
475 isotope composition than the basalts from the north-central Galápagos (where the pyroxenitic  
476 source component is most strongly expressed). As a result, the presence of one or more isotopically  
477 enriched south-western peridotite components are required (Fig. 8), alongside a pyroxenite source  
478 component that is focused beneath the north-central Galápagos and an isotopically depleted north-  
479 eastern peridotite (Fig. 10).

480 As indicated above, we cannot exclude the possibility that a small fraction of pyroxenitic material  
481 (i.e., <5%) exists in the mantle source of all Galápagos basalts and contributes to their isotopic  
482 compositions (Fig. 8). However, the analysis presented here clearly shows that this pyroxenitic  
483 component is present in much higher proportions in the mantle source region of the north-central  
484 Galápagos basalts, separating the isotopically enriched domain of the south-western Galápagos from  
485 the isotopically depleted eastern Galápagos.

## 486 6 IMPLICATIONS FOR THE STRUCTURE OF THE DEEP MANTLE

---

487 Owing to the location of the Galápagos Archipelago above the eastern margin of the Pacific LLSVP,  
488 and the asymmetric structure of the Galápagos mantle plume (with regards to isotopic composition),  
489 it is hypothesised that the plume stem is rooted at the eastern boundary of the Pacific LLSVP (Harpp  
490 and Weis, 2020; Jackson et al., 2018; Ritsema et al., 2011; Fig. 1). Therefore, placing constraints on  
491 the spatial distribution of lithologically distinct components in the Galápagos mantle plume, as  
492 achieved above, can be used to identify the contribution of recycled material to the deep mantle.  
493 Seismic tomography reveals that the structure and slope of the LLSVP boundaries are not uniform  
494 (Cottaar and Lekic, 2016). For example, the boundary of the eastern Pacific LLSVP near the base of  
495 the Galápagos mantle plume is relatively steep (>60°), displaying a sharp transition between the  
496 LLSVP and seismically faster material to the east (Fig. 1; Frost and Rost, 2014). Conversely, the  
497 northern boundary of the Pacific LLSVP, which may represent the source region of the Hawaiian  
498 mantle plume (Weis et al., 2011), is shallower (~25-35°; Frost and Rost, 2014). These variations in the  
499 slope of the LLSVP margins have been hypothesized to result from changes in mantle dynamics and,  
500 specifically, the presence of recycled slabs in the Earth's mantle (Frost and Rost, 2014). Steeper  
501 margins, such as that observed at the eastern margin of the Pacific LLSVP, are attributed to the  
502 presence of subducted slabs, which push into the LLSVP and cause an increased thermal and  
503 compositional gradient. Additionally, a compilation of seismic tomography models indicate that  
504 there is considerable evidence to suggest that recycled slabs are present in the Earth's lowermost

505 mantle beneath the eastern margin of the Pacific Ocean (Cottaar and Lekic, 2016; Shephard et al.,  
506 2017).

507 The distribution of lithologically distinct components in the Galápagos mantle plume allows us to  
508 compare the geochemical signatures of plume-related lavas to these seismic interpretations.

509 Geochemical evidence for pyroxenitic source components is most strongly observed in the  
510 composition of basalts from the volcanoes of northern Isabela (Ecuador and Wolf), Roca Redonda,

511 western Santiago and Santa Cruz. These locations lie along the border between the isotopically  
512 enriched south-western domain and the isotopically depleted north-eastern domain of the

513 Galápagos mantle plume identified by Harpp and Weis (2020). As such, our observations suggest  
514 that the Galápagos mantle plume contains a pyroxenitic, recycled component and that this

515 component is most prevalent within the boundary zone between the enriched LLSVP material to the  
516 south-west and depleted peridotitic mantle to the north-east. It is unclear how the shallow level

517 (<100-200 km depth) deflection of the Galápagos mantle plume to the north-east influences the  
518 projection of spatial variations in basalt chemistry to features in the deep mantle, but, if we assume

519 that the spatial distribution of lower mantle material is maintained during plume ascent (Dannberg  
520 and Gassmöller, 2018; Farnetani et al., 2018), our observations suggest that subducted crustal

521 material is present near the margin of the Pacific LLSVP and is entrained into the core of the  
522 upwelling Galápagos plume (Fig. 11). This distribution of recycled crustal material in the Pacific lower

523 mantle can explain the localized expression of lithological heterogeneity at the surface, and is  
524 consistent with the presence of a seismically fast body near the eastern margin of the Pacific LLSVP

525 (Frost and Rost, 2014).

526 Critically, there is no evidence in either the major element systematics of the Galápagos basalts, or  
527 the minor element contents of their olivine cargo, to indicate that the isotopically enriched LLSVP  
528 material melting beneath the south-western portion of the Galápagos Archipelago is pyroxenitic  
529 (Vidito et al., 2013). Consequently, there is little to no data in the Galápagos to support the popular

530 hypothesis that the LLSVPs represent piles of subducted oceanic crust (Niu, 2018). Notably, our  
531 interpretation that the Pacific LLSVP cannot be dominated by piles of subducted oceanic crust is  
532 consistent with recent ab initio calculations of the density and seismic velocities of subducted crustal  
533 material, which indicate that such bodies should be visible as high velocity regions in the lower  
534 mantle (as opposed to the low seismic velocities of the LLSVPs; Wang et al., 2020). Instead, the  
535 eastern Pacific LLSVP likely contains a contribution from a primordial, or undegassed mantle  
536 component, consistent with the elevated  $^3\text{He}/^4\text{He}$  signature of the Fernandina basalts. In addition,  
537 the isotopic data from the south-western Galápagos and the Loa trend of Hawaii clearly  
538 demonstrate that the LLSVP material is heterogeneous at a range of different length scales, and it is  
539 therefore unlikely that one single process is responsible for the formation of these deep mantle  
540 superstructures (Harpp and Weis, 2020; Jackson et al., 2018).  
  
541 Additionally, our interpretation that recycled crustal components are external to the LLSVPs is  
542 consistent with dynamical models of mantle circulation, which demonstrate that only ~10% of  
543 subducted oceanic crust can be stored in the deep mantle superstructures (Li et al., 2014).  
  
544 Therefore, the distribution of pyroxenitic components in the Galápagos mantle plume demonstrates  
545 that recycled crustal components are present along the eastern margin of the Pacific LLSVP, and  
546 potentially contribute to the steep, sharp transition at the LLSVP margin (Frost and Rost, 2014).

## 547 7 CONCLUSIONS

---

548 The Galápagos Archipelago offers an opportunity to investigate the structure of the Earth's lower  
549 mantle and the origin of the LLSVPs through the geochemical analysis of erupted basalts. In this  
550 study we have used the major element composition of high-MgO basalts, and the minor element  
551 contents of their olivine cargo, to map out the distribution of lithologically distinct components in  
552 the Galápagos mantle plume. By comparing our results with the spatial heterogeneity in the  
553 radiogenic isotope composition of basalts from across the Archipelago we have constrained the

554 distribution of recycled crustal components in the upwelling mantle plume and, by extension, at the  
555 core mantle boundary.

556 Our results indicate that the south-western and north-eastern regions of the Galápagos mantle  
557 plume, corresponding to upwelling LLSVP material and depleted mantle respectively, are dominated  
558 by peridotite, with little evidence for lithological heterogeneity. In the central and northern  
559 Galápagos, however, high FeO<sub>t</sub> contents in primitive basalts, and Fe/Mn ratios >70 in olivine crystals,  
560 provides substantial evidence for the presence of a lithologically distinct, pyroxenitic component in  
561 the mantle source. We interpret this signature to represent the presence of recycled oceanic crust in  
562 the Galápagos mantle plume, likely dragged up from the margins of the Pacific LLSVP. We also note  
563 that there is no evidence in the geochemical composition of the Galápagos basalts to suggest that  
564 upwelling LLSVP material is lithologically distinct from the surrounding mantle. As a result, the Pacific  
565 LLSVP is unlikely to be formed through accumulation of subducted oceanic crust.

## 566 DATA AVAILABILITY STATEMENT

---

567 The data used in this study, and the python scripts used for data plotting, are available via  
568 <https://zenodo.org/badge/latestdoi/384184976>

## 569 ACKNOWLEDGEMENTS

---

570 This study was supported by a NERC (Natural Environmental Research Council) Research Training  
571 Student Grant (NE/L002507/1) and a Research Fellowship funded by the Royal Commission for the  
572 Exhibition of 1851 awarded to M.L.M.G. The Galápagos National Park authorities are acknowledged  
573 for granting SAG permission to undertake fieldwork on Isla Santiago. Staff at CDRS, together with L.  
574 Cruz and his crew, are thanked for logistical support during two field seasons on Isla Santiago. SAG  
575 also thanks those who participated in the fieldwork, including G. Estes, D. Geist, B. Manning-Geist, T.  
576 Grant, A. Miles, D. Norman and A. Thurman. The expeditions were funded by grants to SAG from the  
577 University of Cambridge, Geological Society of London and NERC (RG57434). Finally, we would like to  
578 thank Dennis Geist, William White and an anonymous reviewer for their helpful and constructive  
579 comments on this manuscript.

580

581 REFERENCES

---

- 582 Allan, J.F., Simkin, T., 2000. Fernandina Volcano's evolved, well-mixed basalts: Mineralogical and  
583 petrological constraints on the nature of the Galápagos plume. *J. Geophys. Res. Solid Earth*  
584 105, 6017–6041. <https://doi.org/10.1029/1999JB900417>
- 585 Argus, D.F., Gordon, R.G., DeMets, C., 2011. Geologically current motion of 56 plates relative to the  
586 no-net-rotation reference frame. *Geochem. Geophys. Geosystems* 12.  
587 <https://doi.org/10.1029/2011GC003751>
- 588 Bailey, K., 1976. Potassium-Argon Ages from the Galápagos Islands. *Science* 192, 465–467.  
589 <https://doi.org/10.1126/science.192.4238.465>
- 590 Blichert-Toft, J., White, W.M., 2001. Hf isotope geochemistry of the Galápagos Islands. *Geochem.*  
591 *Geophys. Geosystems* 2. <https://doi.org/10.1029/2000GC000138>
- 592 Bow, C.S., Geist, D.J., 1992. Geology and petrology of Floreana Island, Galápagos Archipelago,  
593 Ecuador. *J. Volcanol. Geotherm. Res.* 52, 83–105. [https://doi.org/10.1016/0377-0273\(92\)90134-Y](https://doi.org/10.1016/0377-0273(92)90134-Y)
- 595 Brandenburg, J.P., van Keken, P.E., 2007. Deep storage of oceanic crust in a vigorously convecting  
596 mantle. *J. Geophys. Res.* 112, B06403. <https://doi.org/10.1029/2006JB004813>
- 597 Canales, J.P., Ito, G., Detrick, R.S., Sinton, J., 2002. Crustal thickness along the western Galápagos  
598 Spreading Center and the compensation of the Galápagos hotspot swell. *Earth Planet. Sci.*  
599 *Lett.* 203, 311–327. [https://doi.org/10.1016/S0012-821X\(02\)00843-9](https://doi.org/10.1016/S0012-821X(02)00843-9)
- 600 Chauvel, C., Hofmann, A.W., Vidal, P., 1992. himu-em: The French Polynesian connection. *Earth*  
601 *Planet. Sci. Lett.* 110, 99–119. [https://doi.org/10.1016/0012-821X\(92\)90042-T](https://doi.org/10.1016/0012-821X(92)90042-T)
- 602 Christie, D.M., Werner, R., Hauff, F., Hoernle, K., Hanan, B.B., 2005. Morphological and geochemical  
603 variations along the eastern Galápagos Spreading Center. *Geochem. Geophys. Geosystems*  
604 6, n/a-n/a. <https://doi.org/10.1029/2004GC000714>
- 605 Cottaar, S., Lekic, V., 2016. Morphology of seismically slow lower-mantle structures. *Geophys. J. Int.*  
606 207, 1122–1136. <https://doi.org/10.1093/gji/ggw324>
- 607 Cushman, B., Sinton, J., Ito, G., Eaby Dixon, J., 2004. Glass compositions, plume-ridge interaction, and  
608 hydrous melting along the Galápagos Spreading Center, 90.5°W to 98°W. *Geochem.*  
609 *Geophys. Geosystems* 5. <https://doi.org/10.1029/2004GC000709>
- 610 Dannberg, J., Gassmöller, R., 2018. Chemical trends in ocean islands explained by plume–slab  
611 interaction. *Proc. Natl. Acad. Sci.* 115, 4351–4356.  
612 <https://doi.org/10.1073/pnas.1714125115>
- 613 Dasgupta, R., Jackson, M.G., Lee, C.-T.A., 2010. Major element chemistry of ocean island basalts —  
614 Conditions of mantle melting and heterogeneity of mantle source. *Earth Planet. Sci. Lett.*  
615 289, 377–392. <https://doi.org/10.1016/j.epsl.2009.11.027>
- 616 Davaille, A., Romanowicz, B., 2020. Deflating the LLSVPs: Bundles of Mantle Thermochemical Plumes  
617 Rather Than Thick Stagnant “Piles.” *Tectonics* 39. <https://doi.org/10.1029/2020TC006265>
- 618 Deschamps, F., Cobden, L., Tackley, P.J., 2012. The primitive nature of large low shear-wave velocity  
619 provinces. *Earth Planet. Sci. Lett.* 349–350, 198–208.  
620 <https://doi.org/10.1016/j.epsl.2012.07.012>
- 621 Detrick, R.S., Sinton, J.M., Ito, G., Canales, J.P., Behn, M., Blacic, T., Cushman, B., Dixon, J.E., Graham,  
622 D.W., Mahoney, J.J., 2002. Correlated geophysical, geochemical, and volcanological  
623 manifestations of plume-ridge interaction along the Galápagos Spreading Center. *Geochem.*  
624 *Geophys. Geosystems* 3, 1–14. <https://doi.org/10.1029/2002GC000350>
- 625 Doubrovine, P.V., Steinberger, B., Torsvik, T.H., 2016. A failure to reject: Testing the correlation  
626 between large igneous provinces and deep mantle structures with EDF statistics. *Geochem.*  
627 *Geophys. Geosystems* 17, 1130–1163. <https://doi.org/10.1002/2015GC006044>
- 628 Dziewonski, A.M., Woodhouse, J.H., 1987. Global Images of the Earth’s Interior. *Science* 236, 37–48.  
629 <https://doi.org/10.1126/science.236.4797.37>

- 630 Farley, K.A., Natland, J.H., Craig, H., 1992. Binary mixing of enriched and undegassed (primitive?)  
631 mantle components (He, Sr, Nd, Pb) in Samoan lavas. *Earth Planet. Sci. Lett.* 111, 183–199.  
632 [https://doi.org/10.1016/0012-821X\(92\)90178-X](https://doi.org/10.1016/0012-821X(92)90178-X)
- 633 Farnetani, C.G., Hofmann, A.W., Duvernay, T., Limare, A., 2018. Dynamics of rheological  
634 heterogeneities in mantle plumes. *Earth Planet. Sci. Lett.* 499, 74–82.  
635 <https://doi.org/10.1016/j.epsl.2018.07.022>
- 636 French, S.W., Romanowicz, B., 2015. Broad plumes rooted at the base of the Earth's mantle beneath  
637 major hotspots 19.
- 638 Frost, D.A., Rost, S., 2014. The P-wave boundary of the Large-Low Shear Velocity Province beneath  
639 the Pacific. *Earth Planet. Sci. Lett.* 403, 380–392. <https://doi.org/10.1016/j.epsl.2014.06.046>
- 640 Garnero, E.J., McNamara, A.K., Shim, S.-H., 2016. Continent-sized anomalous zones with low seismic  
641 velocity at the base of Earth's mantle. *Nat. Geosci.* 9, 481–489.  
642 <https://doi.org/10.1038/ngeo2733>
- 643 Geist, D., White, W.M., Albarede, F., Harpp, K., Reynolds, R., Blichert-Toft, J., Kurz, M.D., 2002.  
644 Volcanic evolution in the Galápagos: The dissected shield of Volcan Ecuador. *Geochem.*  
645 *Geophys. Geosystems* 3, 1 of 32–32 32. <https://doi.org/10.1029/2002GC000355>
- 646 Geist, D.J., Fornari, D.J., Kurz, M.D., Harpp, K.S., Adam Soule, S., Perfit, M.R., Koleszar, A.M., 2006.  
647 Submarine Fernandina: Magmatism at the leading edge of the Galápagos hot spot.  
648 *Geochem. Geophys. Geosystems* 7. <https://doi.org/10.1029/2006GC001290>
- 649 Geist, D.J., McBIRNEY, A.R., Duncan, R.A., 1986. Geology and petrogenesis of lavas from San  
650 Cristobal Island, Galápagos Archipelago. *Geol. Soc. Am. Bull.* 97, 555.  
651 [https://doi.org/10.1130/0016-7606\(1986\)97<555:GAPOLF>2.0.CO;2](https://doi.org/10.1130/0016-7606(1986)97<555:GAPOLF>2.0.CO;2)
- 652 Geist, D.J., Naumann, T.R., Standish, J.J., Kurz, M.D., Harpp, K.S., White, W.M., Fornari, D.J., 2005.  
653 Wolf Volcano, Galápagos Archipelago: Melting and Magmatic Evolution at the Margins of a  
654 Mantle Plume. *J. Petrol.* 46, 2197–2224. <https://doi.org/10.1093/petrology/egi052>
- 655 Geist, D.J., White, W.M., McBirney, A.R., 1988. Plume-asthenosphere mixing beneath the Galápagos  
656 archipelago. *Nature* 333, 657–660. <https://doi.org/10.1038/333657a0>
- 657 Gibson, S.A., 2002. Major element heterogeneity in Archean to Recent mantle plume starting-heads.  
658 *Earth Planet. Sci. Lett.* 195, 59–74. [https://doi.org/10.1016/S0012-821X\(01\)00566-0](https://doi.org/10.1016/S0012-821X(01)00566-0)
- 659 Gibson, S.A., Dale, C.W., Geist, D.J., Day, J.A., Brügmann, G., Harpp, K.S., 2016. The influence of melt  
660 flux and crustal processing on Re–Os isotope systematics of ocean island basalts: Constraints  
661 from Galápagos. *Earth Planet. Sci. Lett.* 449, 345–359.  
662 <https://doi.org/10.1016/j.epsl.2016.05.021>
- 663 Gibson, S.A., Geist, D., 2010. Geochemical and geophysical estimates of lithospheric thickness  
664 variation beneath Galápagos. *Earth Planet. Sci. Lett.* 300, 275–286.  
665 <https://doi.org/10.1016/j.epsl.2010.10.002>
- 666 Gibson, S.A., Geist, D.G., Day, J.A., Dale, C.W., 2012. Short wavelength heterogeneity in the  
667 Galápagos plume: Evidence from compositionally diverse basalts on Isla Santiago. *Geochem.*  
668 *Geophys. Geosystems* 13. <https://doi.org/10.1029/2012GC004244>
- 669 Gibson, S.A., Geist, D.J., Richards, M.A., 2015. Mantle plume capture, anchoring, and outflow during  
670 Galápagos plume-ridge interaction: Mantle plume capture & outflow. *Geochem. Geophys.*  
671 *Geosystems* 16, 1634–1655. <https://doi.org/10.1002/2015GC005723>
- 672 Gibson, S.A., Richards, M.A., 2018. Delivery of deep-sourced, volatile-rich plume material to the  
673 global ridge system. *Earth Planet. Sci. Lett.* 499, 205–218.  
674 <https://doi.org/10.1016/j.epsl.2018.07.028>
- 675 Gibson, S.A., Thompson, R.N., Dickin, A.P., 2000. Ferropicrites: geochemical evidence for Fe-rich  
676 streaks in upwelling mantle plumes. *Earth Planet. Sci. Lett.* 174, 355–374.  
677 [https://doi.org/10.1016/S0012-821X\(99\)00274-5](https://doi.org/10.1016/S0012-821X(99)00274-5)
- 678 Gleeson, M., Gibson, S., 2021. Insights into the nature of plume-ridge interaction and outflux of H<sub>2</sub>O  
679 from the Galápagos Spreading Centre (preprint). *Earth Sciences*.  
680 <https://doi.org/10.31223/X57P5C>

- 681 Gleeson, M.L.M., Gibson, S.A., 2019. Crustal controls on apparent mantle pyroxenite signals in  
682 ocean-island basalts. *Geology*. <https://doi.org/10.1130/G45759.1>
- 683 Gleeson, Matthew L M, Gibson, S.A., Stock, M.J., 2020. Upper mantle mush zones beneath low melt  
684 flux ocean island volcanoes: insights from Isla Floreana, Galápagos. *J. Petrol.* egaa094.  
685 <https://doi.org/10.1093/petrology/egaa094>
- 686 Gleeson, Matthew L.M., Gibson, S.A., Williams, H.M., 2020. Novel insights from Fe-isotopes into the  
687 lithological heterogeneity of Ocean Island Basalts and plume-influenced MORBs. *Earth*  
688 *Planet. Sci. Lett.* 535, 116114. <https://doi.org/10.1016/j.epsl.2020.116114>
- 689 Global Volcanism Program, 2013. Volcanoes of the World, v. 4.3.4.
- 690 Gurenko, A.A., Geldmacher, J., Hoernle, K.A., Sobolev, A.V., 2013. A composite, isotopically-depleted  
691 peridotite and enriched pyroxenite source for Madeira magmas: Insights from olivine. *Lithos*  
692 170–171, 224–238. <https://doi.org/10.1016/j.lithos.2013.03.002>
- 693 Gurenko, A.A., Sobolev, A.V., Hoernle, K.A., Hauff, F., Schmincke, H.-U., 2009. Enriched, HIMU-type  
694 peridotite and depleted recycled pyroxenite in the Canary plume: A mixed-up mantle. *Earth*  
695 *Planet. Sci. Lett.* 277, 514–524. <https://doi.org/10.1016/j.epsl.2008.11.013>
- 696 Hanan, B.B., Graham, D.W., 1996. Lead and Helium Isotope Evidence from Oceanic Basalts for a  
697 Common Deep Source of Mantle Plumes. *Science* 272, 991–995.  
698 <https://doi.org/10.1126/science.272.5264.991>
- 699 Harpp, K.S., Fornari, D.J., Geist, D.J., Kurz, M.D., 2003. Genovesa Submarine Ridge: A manifestation  
700 of plume-ridge interaction in the northern Galápagos Islands. *Geochem. Geophys.*  
701 *Geosystems* 4. <https://doi.org/10.1029/2003GC000531>
- 702 Harpp, K.S., Geist, D.J., Koleszar, A.M., Christensen, B., Lyons, J., Sabga, M., Rollins, N., 2014a. The  
703 Geology and Geochemistry of Isla Floreana, Galápagos: A Different Type of Late-Stage Ocean  
704 Island Volcanism, in: Harpp, K.S., Mittelstaedt, E., d’Ozouville, N., Graham, D.W. (Eds.),  
705 *Geophysical Monograph Series*. John Wiley & Sons, Inc, Hoboken, New Jersey, pp. 71–117.  
706 <https://doi.org/10.1002/9781118852538.ch6>
- 707 Harpp, K.S., Hall, P.S., Jackson, M.G., 2014b. Galápagos and Easter: A Tale of Two Hotspots, in:  
708 Harpp, K.S., Mittelstaedt, E., d’Ozouville, N., Graham, D.W. (Eds.), *Geophysical Monograph*  
709 *Series*. John Wiley & Sons, Inc, Hoboken, New Jersey, pp. 27–40.  
710 <https://doi.org/10.1002/9781118852538.ch3>
- 711 Harpp, K.S., Weis, D., 2020. Insights Into the Origins and Compositions of Mantle Plumes: A  
712 Comparison of Galápagos and Hawai’i. *Geochem. Geophys. Geosystems* 21.  
713 <https://doi.org/10.1029/2019GC008887>
- 714 Harpp, K.S., White, W.M., 2001. Tracing a mantle plume: Isotopic and trace element variations of  
715 Galápagos seamounts. *Geochem. Geophys. Geosystems* 2, n/a-n/a.  
716 <https://doi.org/10.1029/2000GC000137>
- 717 Hauri, E.H., 1996. Major-element variability in the Hawaiian mantle plume. *Nature* 382, 415–419.  
718 <https://doi.org/10.1038/382415a0>
- 719 Herzberg, C., 2011. Identification of Source Lithology in the Hawaiian and Canary Islands:  
720 Implications for Origins. *J. Petrol.* 52, 113–146. <https://doi.org/10.1093/petrology/egq075>
- 721 Herzberg, C., Asimow, P.D., 2008. Petrology of some oceanic island basalts: PRIMELT2.XLS software  
722 for primary magma calculation. *Geochem. Geophys. Geosystems* 9, n/a-n/a.  
723 <https://doi.org/10.1029/2008GC002057>
- 724 Herzberg, C., Cabral, R.A., Jackson, M.G., Vidito, C., Day, J.M.D., Hauri, E.H., 2014. Phantom Archean  
725 crust in Mangaia hotspot lavas and the meaning of heterogeneous mantle. *Earth Planet. Sci.*  
726 *Lett.* 396, 97–106. <https://doi.org/10.1016/j.epsl.2014.03.065>
- 727 Herzberg, C., O’Hara, M.J., 2002. Plume-Associated Ultramafic Magmas of Phanerozoic Age. *J. Petrol.*  
728 43, 1857–1883. <https://doi.org/10.1093/petrology/43.10.1857>
- 729 Heyn, B.H., Conrad, C.P., Trønnes, R.G., 2020. How Thermochemical Piles Can (Periodically) Generate  
730 Plumes at Their Edges. *J. Geophys. Res. Solid Earth* 125.  
731 <https://doi.org/10.1029/2019JB018726>

- 732 Hirose, K., Kushiro, I., 1993. Partial melting of dry peridotites at high pressures: Determination of  
733 compositions of melts segregated from peridotite using aggregates of diamond. *Earth*  
734 *Planet. Sci. Lett.* 114, 477–489. [https://doi.org/10.1016/0012-821X\(93\)90077-M](https://doi.org/10.1016/0012-821X(93)90077-M)
- 735 Hirschmann, M.M., Kogiso, Tetsu, Baker, M.B., Stolper, E.M., 2003. Alkalic magmas generated by  
736 partial melting of garnet pyroxenite 4.
- 737 Hoernle, K., Rohde, J., Hauff, F., Garbe-Schönberg, D., Homrighausen, S., Werner, R., Morgan, J.P.,  
738 2015. How and when plume zonation appeared during the 132 Myr evolution of the Tristan  
739 Hotspot. *Nat. Commun.* 6, 7799. <https://doi.org/10.1038/ncomms8799>
- 740 Hoernle, K., Werner, R., Morgan, J.P., Garbe-Schönberg, D., Bryce, J., Mrazek, J., 2000. Existence of  
741 complex spatial zonation in the Galápagos plume. *Geology* 28, 435.  
742 [https://doi.org/10.1130/0091-7613\(2000\)28<435:EOCSZI>2.0.CO;2](https://doi.org/10.1130/0091-7613(2000)28<435:EOCSZI>2.0.CO;2)
- 743 Hofmann, A.W., 1997. Mantle geochemistry: the message from oceanic volcanism. *Nature* 385, 219–  
744 229. <https://doi.org/10.1038/385219a0>
- 745 Holland, T.J.B., Green, E.C.R., Powell, R., 2018. Melting of Peridotites through to Granites: A Simple  
746 Thermodynamic Model in the System KNCFMASHTOCr. *J. Petrol.* 59, 881–900.  
747 <https://doi.org/10.1093/petrology/egy048>
- 748 Holland, T.J.B., Powell, R., 2011. An improved and extended internally consistent thermodynamic  
749 dataset for phases of petrological interest, involving a new equation of state for solids. *J.*  
750 *Metamorph. Geol.* 29, 333–383. <https://doi.org/10.1111/j.1525-1314.2010.00923.x>
- 751 Hooft, E.E.E., Toomey, D.R., Solomon, S.C., 2003. Anomalously thin transition zone beneath the  
752 Galápagos hotspot. *Earth Planet. Sci. Lett.* 216, 55–64. [https://doi.org/10.1016/S0012-821X\(03\)00517-X](https://doi.org/10.1016/S0012-821X(03)00517-X)
- 753 Huang, S., Hall, P.S., Jackson, M.G., 2011. Geochemical zoning of volcanic chains associated with  
754 Pacific hotspots. *Nat. Geosci.* 4, 874–878. <https://doi.org/10.1038/ngeo1263>
- 755 Humayun, M., Qin, L., Norman, M., 2004. Geochemical Evidence for Excess Iron in the Mantle  
756 Beneath Hawaii. *Science* 306, 91–94. <https://doi.org/10.1126/science.1101050>
- 757 Ingle, S., Ito, G., Mahoney, J.J., Chazey, W., Sinton, J., Rotella, M., Christie, D.M., 2010. Mechanisms  
758 of geochemical and geophysical variations along the western Galápagos Spreading Center.  
759 *Geochem. Geophys. Geosystems* 11. <https://doi.org/10.1029/2009GC002694>
- 760 Jackson, M.G., Becker, T.W., Konter, J.G., 2018. Geochemistry and Distribution of Recycled Domains  
761 in the Mantle Inferred From Nd and Pb Isotopes in Oceanic Hot Spots: Implications for  
762 Storage in the Large Low Shear Wave Velocity Provinces. *Geochem. Geophys. Geosystems*  
763 19, 3496–3519. <https://doi.org/10.1029/2018GC007552>
- 764 Jackson, M.G., Carlson, R.W., Kurz, M.D., Kempton, P.D., Francis, D., Blusztajn, J., 2010. Evidence for  
765 the survival of the oldest terrestrial mantle reservoir. *Nature* 466, 853–856.  
766 <https://doi.org/10.1038/nature09287>
- 767 Kogiso, T., Hirschmann, M.M., Frost, D.J., 2003. High-pressure partial melting of garnet pyroxenite:  
768 possible mafic lithologies in the source of ocean island basalts. *Earth Planet. Sci. Lett.* 216,  
769 603–617. [https://doi.org/10.1016/S0012-821X\(03\)00538-7](https://doi.org/10.1016/S0012-821X(03)00538-7)
- 770 Kurz, M.D., Geist, D., 1999. Dynamics of the Galápagos hotspot from helium isotope geochemistry.  
771 *Geochim. Cosmochim. Acta* 63, 4139–4156. [https://doi.org/10.1016/S0016-7037\(99\)00314-2](https://doi.org/10.1016/S0016-7037(99)00314-2)
- 772 Labrosse, S., Hernlund, J.W., Coltice, N., 2007. A crystallizing dense magma ocean at the base of the  
773 Earth's mantle. *Nature* 450, 866–869. <https://doi.org/10.1038/nature06355>
- 774 Lambart, S., 2017. No direct contribution of recycled crust in Icelandic basalts. *Geochem. Perspect.*  
775 *Lett.* 7–12. <https://doi.org/10.7185/geochemlet.1728>
- 776 Lambart, S., Baker, M.B., Stolper, E.M., 2016. The role of pyroxenite in basalt genesis: Melt-PX, a  
777 melting parameterization for mantle pyroxenites between 0.9 and 5 GPa: Melt-PX:  
778 Pyroxenite Melting Model. *J. Geophys. Res. Solid Earth* 121, 5708–5735.  
779 <https://doi.org/10.1002/2015JB012762>
- 780
- 781

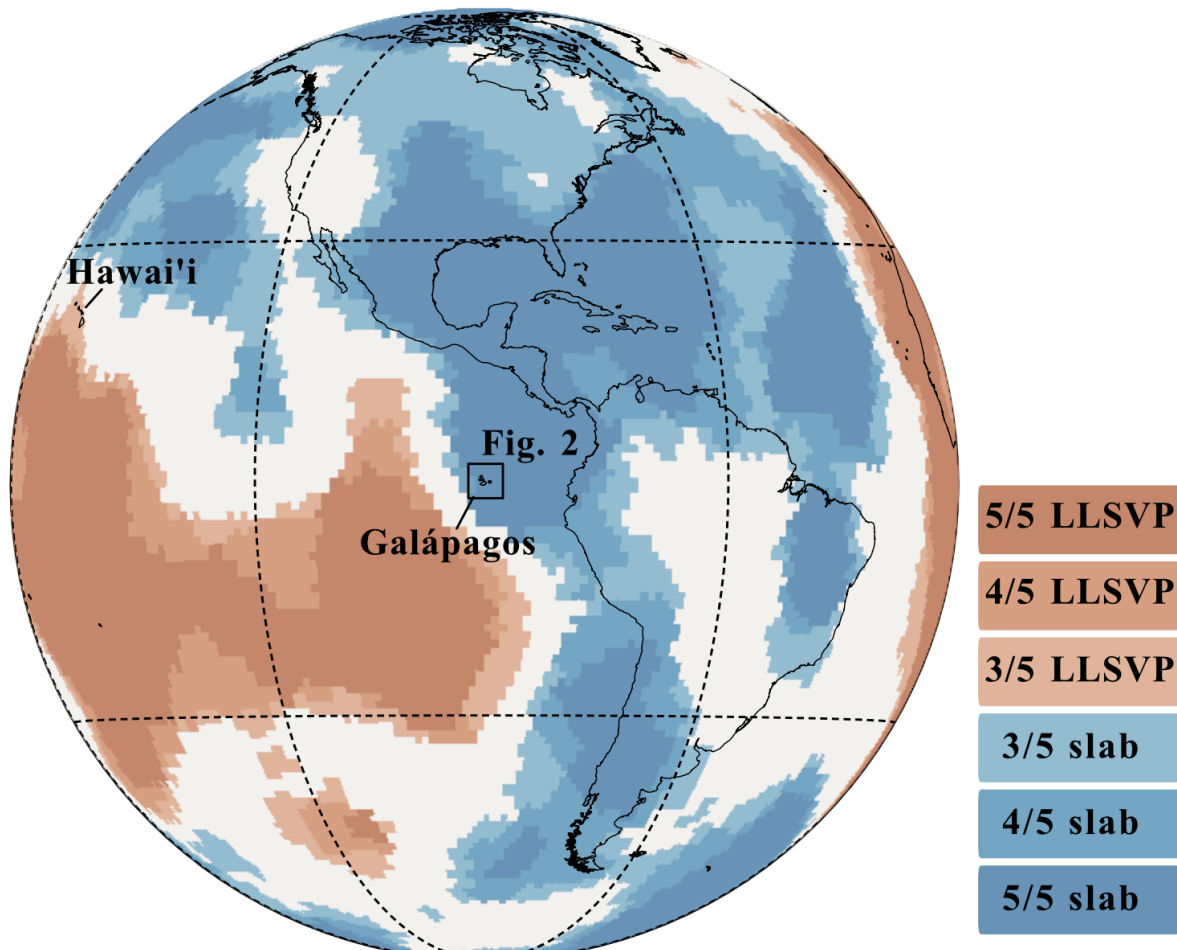
- 782 Lambart, S., Laporte, D., Provost, A., Schiano, P., 2012. Fate of Pyroxenite-derived Melts in the  
783 Peridotitic Mantle: Thermodynamic and Experimental Constraints. *J. Petrol.* 53, 451–476.  
784 <https://doi.org/10.1093/petrology/egr068>
- 785 Lambart, S., Laporte, D., Schiano, P., 2013. Markers of the pyroxenite contribution in the major-  
786 element compositions of oceanic basalts: Review of the experimental constraints. *Lithos*  
787 160–161, 14–36. <https://doi.org/10.1016/j.lithos.2012.11.018>
- 788 Lau, H.C.P., Mitrovica, J.X., Davis, J.L., Tromp, J., Yang, H.-Y., Al-Attar, D., 2017. Tidal tomography  
789 constrains Earth's deep-mantle buoyancy. *Nature* 551, 321–326.  
790 <https://doi.org/10.1038/nature24452>
- 791 Li, M., McNamara, A.K., Garnero, E.J., 2014. Chemical complexity of hotspots caused by cycling  
792 oceanic crust through mantle reservoirs. *Nat. Geosci.* 7, 366–370.  
793 <https://doi.org/10.1038/ngeo2120>
- 794 Mahr, J., Harpp, K.S., Kurz, M.D., Geist, D., Bercovici, H., Pimentel, R., Cleary, Z., 2016. Rejuvenescent  
795 Volcanism on San Cristóbal Island, Galápagos: A Late "Plumer". *AGU Fall Abstr.*
- 796 Mallik, A., Dasgupta, R., 2012. Reaction between MORB-eclogite derived melts and fertile peridotite  
797 and generation of ocean island basalts. *Earth Planet. Sci. Lett.* 329–330, 97–108.  
798 <https://doi.org/10.1016/j.epsl.2012.02.007>
- 799 Matthews, S., Shorttle, O., Wong, K., 2020. *simonwmatthews/pyMelt*: First Release. *Zenodo*.  
800 <https://doi.org/10.5281/ZENODO.4011814>
- 801 Matthews, S., Wong, K., Shorttle, O., Edmonds, M., MacLennan, J., 2021. Do Olivine Crystallization  
802 Temperatures Faithfully Record Mantle Temperature Variability? *Geochem. Geophys.*  
803 *Geosystems* 22. <https://doi.org/10.1029/2020GC009157>
- 804 Matzen, A.K., Baker, M.B., Beckett, J.R., Stolper, E.M., 2013. The Temperature and Pressure  
805 Dependence of Nickel Partitioning between Olivine and Silicate Melt. *J. Petrol.* 54, 2521–  
806 2545. <https://doi.org/10.1093/petrology/egt055>
- 807 Matzen, A.K., Baker, M.B., Beckett, J.R., Wood, B.J., Stolper, E.M., 2017b. The effect of liquid  
808 composition on the partitioning of Ni between olivine and silicate melt. *Contrib. Mineral.*  
809 *Petrol.* 172. <https://doi.org/10.1007/s00410-016-1319-8>
- 810 Matzen, A.K., Wood, B.J., Baker, M.B., Stolper, E.M., 2017a. The roles of pyroxenite and peridotite in  
811 the mantle sources of oceanic basalts. *Nat. Geosci.* 10, 530–535.  
812 <https://doi.org/10.1038/ngeo2968>
- 813 McBirney, A., Williams, H., 1969. Geology and Petrology of the Galápagos Islands. *Geological Society*  
814 *of America*.
- 815 Morgan, W.J., 1971. Convection Plumes in the Lower Mantle. *Nature* 230, 42–43.  
816 <https://doi.org/10.1038/230042a0>
- 817 Moulik, P., Ekström, G., 2016. The relationships between large-scale variations in shear velocity,  
818 density, and compressional velocity in the Earth's mantle: LARGE-SCALE  $v_p$ ,  $v_s$ , AND  $\rho$   
819 VARIATIONS. *J. Geophys. Res. Solid Earth* 121, 2737–2771.  
820 <https://doi.org/10.1002/2015JB012679>
- 821 Naumann, T., 2002. Petrology and Geochemistry of Volcan Cerro Azul: Petrologic Diversity among  
822 the Western Galápagos Volcanoes. *J. Petrol.* 43, 859–883.  
823 <https://doi.org/10.1093/petrology/43.5.859>
- 824 Naumann, T., Geist, D., 2000. Physical volcanology and structural development of Cerro Azul  
825 Volcano, Isabela Island, Galápagos: implications for the development of Galápagos-type  
826 shield volcanoes. *Bull. Volcanol.* 61, 497–514. <https://doi.org/10.1007/s004450050001>
- 827 Niu, Y., 2018. Origin of the LLSVPs at the base of the mantle is a consequence of plate tectonics – A  
828 petrological and geochemical perspective. *Geosci. Front.* 9, 1265–1278.  
829 <https://doi.org/10.1016/j.gsf.2018.03.005>
- 830 Nolet, G., Hello, Y., Lee, S. van der, Bonnieux, S., Ruiz, M.C., Pazmino, N.A., Deschamps, A., Regnier,  
831 M.M., Font, Y., Chen, Y.J., Simons, F.J., 2019. Imaging the Galápagos mantle plume with an

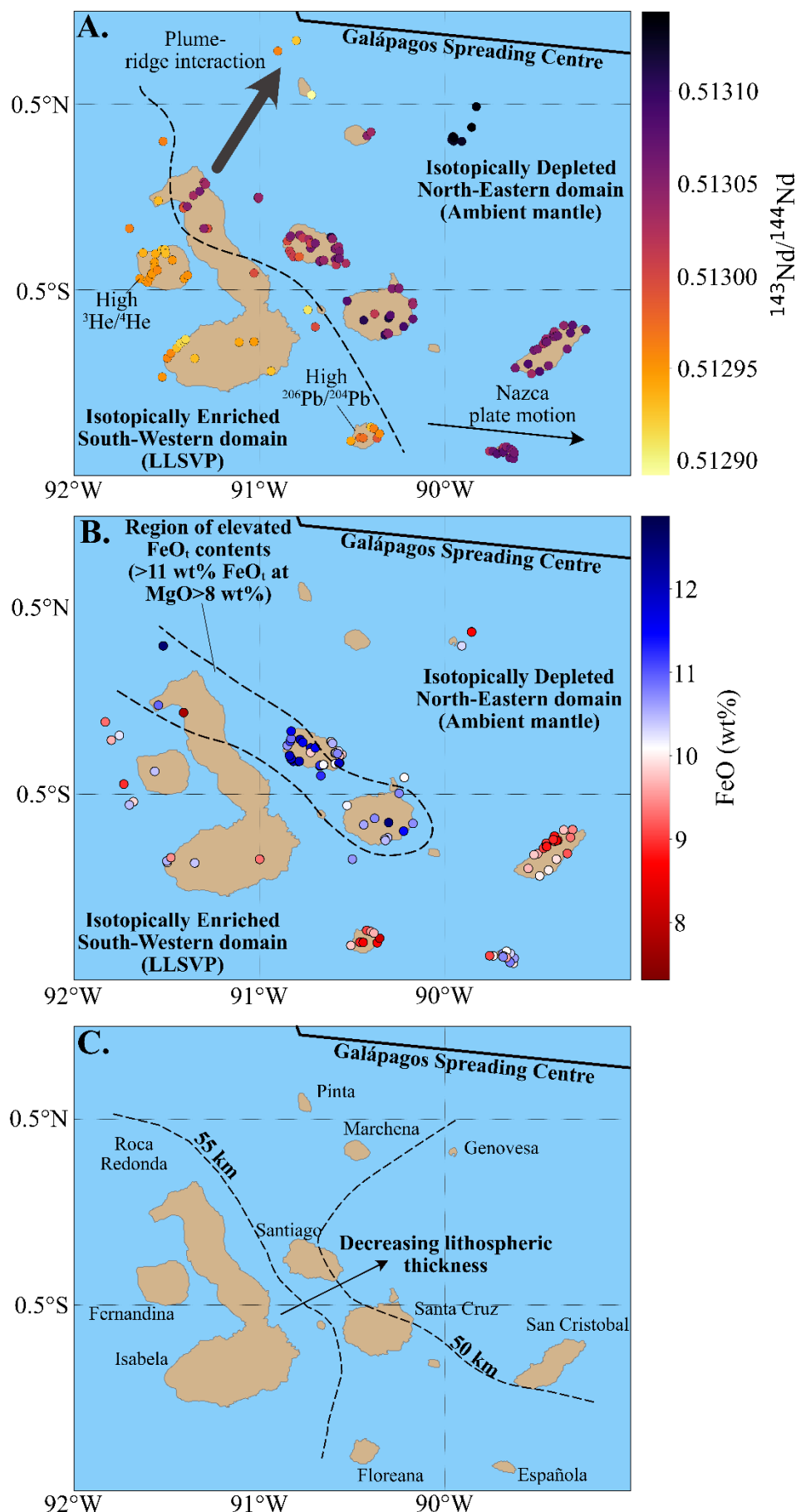
- 832 unconventional application of floating seismometers. *Sci. Rep.* 9, 1326.  
833 <https://doi.org/10.1038/s41598-018-36835-w>
- 834 Peters, B.J., Carlson, R.W., Day, J.M.D., Horan, M.F., 2018. Hadean silicate differentiation preserved  
835 by anomalous  $^{142}\text{Nd}/^{144}\text{Nd}$  ratios in the Réunion hotspot source. *Nature* 555, 89–93.  
836 <https://doi.org/10.1038/nature25754>
- 837 Powell, R., Holland, T., Worley, B., 1998. Calculating phase diagrams involving solid solutions via non-  
838 linear equations, with examples using THERMOCALC. *J. Metamorph. Geol.* 16, 577–588.  
839 <https://doi.org/10.1111/j.1525-1314.1998.00157.x>
- 840 Richards, F., Hoggard, M., Ghelichkhan, S., Koelemeijer, P., Lau, H., 2021. Geodynamic, geodetic, and  
841 seismic constraints favour deflated and dense-cored LLVPs (preprint). *Cosmochemistry*.  
842 <https://doi.org/10.31223/X55601>
- 843 Ritsema, J., Deuss, A., van Heijst, H.J., Woodhouse, J.H., 2011. S40RTS: a degree-40 shear-velocity  
844 model for the mantle from new Rayleigh wave dispersion, teleseismic traveltimes and  
845 normal-mode splitting function measurements. *Geophys. J. Int.* 184, 1223–1236.  
846 <https://doi.org/10.1111/j.1365-246X.2010.04884.x>
- 847 Rosenthal, A., Yaxley, G.M., Green, D.H., Hermann, J., Kovács, I., Spandler, C., 2015. Continuous  
848 eclogite melting and variable refertilisation in upwelling heterogeneous mantle. *Sci. Rep.* 4.  
849 <https://doi.org/10.1038/srep06099>
- 850 Rychert, C.A., Harmon, N., Ebinger, C., 2014. Receiver function imaging of lithospheric structure and  
851 the onset of melting beneath the Galápagos Archipelago. *Earth Planet. Sci. Lett.* 388, 156–  
852 165. <https://doi.org/10.1016/j.epsl.2013.11.027>
- 853 Saal, A., Kurz, M., Hart, S., Blusztajn, J., Blicherttoft, J., Liang, Y., Geist, D., 2007. The role of  
854 lithospheric gabbros on the composition of Galápagos lavas. *Earth Planet. Sci. Lett.* 257,  
855 391–406. <https://doi.org/10.1016/j.epsl.2007.02.040>
- 856 Schilling, J.-G., Kingsley, R.H., Devine, J.D., 1982. Galápagos Hot Spot-Spreading Center System: 1.  
857 Spatial petrological and geochemical variations ( $83^\circ\text{W}$ - $101^\circ\text{W}$ ). *J. Geophys. Res. Solid Earth*  
858 87, 5593–5610. <https://doi.org/10.1029/JB087iB07p05593>
- 859 Shephard, G.E., Matthews, K.J., Hosseini, K., Domeier, M., 2017. On the consistency of seismically  
860 imaged lower mantle slabs. *Sci. Rep.* 7, 10976. <https://doi.org/10.1038/s41598-017-11039-w>
- 861 Shorttle, O., MacLennan, J., 2011. Compositional trends of Icelandic basalts: Implications for short-  
862 length scale lithological heterogeneity in mantle plumes. *Geochem. Geophys. Geosystems*  
863 12. <https://doi.org/10.1029/2011GC003748>
- 864 Shorttle, O., MacLennan, J., Lambart, S., 2014. Quantifying lithological variability in the mantle. *Earth*  
865 *Planet. Sci. Lett.* 395, 24–40. <https://doi.org/10.1016/j.epsl.2014.03.040>
- 866 Sinton, J., Detrick, R., Canales, J.P., Ito, G., Behn, M., 2003. Morphology and segmentation of the  
867 western Galápagos Spreading Center,  $90.5^\circ$ - $98^\circ\text{W}$ : Plume-ridge interaction at an  
868 intermediate spreading ridge. *Geochem. Geophys. Geosystems* 4.  
869 <https://doi.org/10.1029/2003GC000609>
- 870 Sobolev, A.V., Hofmann, A.W., Kuzmin, D.V., Yaxley, G.M., Arndt, N.T., Chung, S.-L., Danyushevsky,  
871 L.V., Elliott, T., Frey, F.A., Garcia, M.O., Gurenko, A.A., Kamenetsky, V.S., Kerr, A.C.,  
872 Krivolutskaya, N.A., Matvienkov, V.V., Nikogosian, I.K., Rocholl, A., Sigurdsson, I.A.,  
873 Sushchevskaya, N.M., Teklay, M., 2007. The Amount of Recycled Crust in Sources of Mantle-  
874 Derived Melts 316, 7.
- 875 Sobolev, A.V., Hofmann, A.W., Sobolev, S.V., Nikogosian, I.K., 2005. An olivine-free mantle source of  
876 Hawaiian shield basalts. *Nature* 434, 590–597. <https://doi.org/10.1038/nature03411>
- 877 Standish, J., Geist, D., Harpp, K., Kurz, M.D., 1998. The emergence of a Galápagos shield volcano,  
878 Roca Redonda. *Contrib. Mineral. Petrol.* 133, 136–148.  
879 <https://doi.org/10.1007/s004100050443>
- 880 Steinberger, B., Seidel, M., Torsvik, T.H., 2017. Limited true polar wander as evidence that Earth's  
881 nonhydrostatic shape is persistently triaxial. *Geophys. Res. Lett.* 44, 827–834.  
882 <https://doi.org/10.1002/2016GL071937>

- 883 Stevenson D.S. (2019) Planetary Tectonism. In: Red Dwarfs. Springer, Cham.  
884 [https://doi.org/10.1007/978-3-030-25550-3\\_3](https://doi.org/10.1007/978-3-030-25550-3_3)
- 885 Stracke, A., Hofmann, A.W., Hart, S.R., 2005. FOZO, HIMU, and the rest of the mantle zoo. *Geochem.*  
886 *Geophys. Geosystems* 6. <https://doi.org/10.1029/2004GC000824>
- 887 Stuart, F.M., Lass-Evans, S., Godfrey Fitton, J., Ellam, R.M., 2003. High  $^{3}\text{He}/^{4}\text{He}$  ratios in picritic  
888 basalts from Baffin Island and the role of a mixed reservoir in mantle plumes. *Nature* 424,  
889 57–59. <https://doi.org/10.1038/nature01711>
- 890 Swanson, F., Baitis, H., Lexa, J., Dymond, J., 1974. Geology of Santiago, Rábida, and Pinzón Islands,  
891 Galápagos. *GSA Bull.* [https://doi.org/10.1130/0016-7606\(1974\)85%3C1803:GOSRAP%3E2.0.CO;2](https://doi.org/10.1130/0016-7606(1974)85%3C1803:GOSRAP%3E2.0.CO;2)
- 892 Takahashi, E., Shimazaki, T., Tsuzaki, Y., Yoshida, H., 1993. Melting study of a peridotite KLB-1 to 6.5  
893 GPa, and the origin of basaltic magmas. *Philos. Trans. R. Soc. Lond. Ser. Phys. Eng. Sci.* 342,  
894 105–120. <https://doi.org/10.1098/rsta.1993.0008>
- 895 Teasdale, R., Geist, D., Kurz, M., Harpp, K., 2005. 1998 Eruption at Volcán Cerro Azul, Galápagos  
896 Islands: I. Syn-Eruptive Petrogenesis. *Bull. Volcanol.* 67, 170–185.  
897 <https://doi.org/10.1007/s00445-004-0371-9>
- 898 Trela, J., Vidito, C., Gazel, E., Herzberg, C., Class, C., Whalen, W., Jicha, B., Bizimis, M., Alvarado, G.E.,  
899 2015. Recycled crust in the Galápagos Plume source at 70 Ma: Implications for plume  
900 evolution. *Earth Planet. Sci. Lett.* 425, 268–277. <https://doi.org/10.1016/j.epsl.2015.05.036>
- 901 Vidito, C., Herzberg, C., Gazel, E., Geist, D., Harpp, K., 2013. Lithological structure of the Galápagos  
902 Plume. *Geochem. Geophys. Geosystems* 14, 4214–4240.  
903 <https://doi.org/10.1002/ggge.20270>
- 904 Villagómez, D.R., Toomey, D.R., Geist, D.J., Hooft, E.E.E., Solomon, S.C., 2014. Mantle flow and  
905 multistage melting beneath the Galápagos hotspot revealed by seismic imaging. *Nat. Geosci.*  
906 7, 151–156. <https://doi.org/10.1038/ngeo2062>
- 907 Wang, W., Xu, Y., Sun, D., Ni, S., Wentzcovitch, R., Wu, Z., 2020. Velocity and density characteristics  
908 of subducted oceanic crust and the origin of lower-mantle heterogeneities. *Nat. Commun.*  
909 11, 64. <https://doi.org/10.1038/s41467-019-13720-2>
- 910 Weis, D., Garcia, M.O., Rhodes, J.M., Jellinek, M., Scoates, J.S., 2011. Role of the deep mantle in  
911 generating the compositional asymmetry of the Hawaiian mantle plume. *Nat. Geosci.* 4,  
912 831–838. <https://doi.org/10.1038/ngeo1328>
- 913 White, W.M., Hofmann, A.W., 1982. Sr and Nd isotope geochemistry of oceanic basalts and mantle  
914 evolution. *Nature* 296, 821–825. <https://doi.org/10.1038/296821a0>
- 915 White, W.M., McBirney, A.R., Duncan, R.A., 1993. Petrology and geochemistry of the Galápagos  
916 Islands: Portrait of a pathological mantle plume. *J. Geophys. Res. Solid Earth* 98, 19533–  
917 19563. <https://doi.org/10.1029/93JB02018>
- 918 Wieser, P.E., Edmonds, M., MacLennan, J., Jenner, F.E., Kunz, B.E., 2019. Crystal scavenging from  
919 mush piles recorded by melt inclusions. *Nat Commun* 10, 5797.  
920 <https://doi.org/10.1038/s41467-019-13518-2>
- 921 Willbold, M., Stracke, A., 2006. Trace element composition of mantle end-members: Implications for  
922 recycling of oceanic and upper and lower continental crust. *Geochem. Geophys. Geosystems*  
923 7, n/a-n/a. <https://doi.org/10.1029/2005GC001005>
- 924 Wilson, J.T., 1973. Mantle plumes and plate motions. *Tectonophysics* 19, 149–164.  
925 [https://doi.org/10.1016/0040-1951\(73\)90037-1](https://doi.org/10.1016/0040-1951(73)90037-1)
- 926 Yaxley, G.M., Green, D.H., 1998. Reactions between eclogite and peridotite: mantle refertilisation by  
927 subduction of oceanic crust. *Schweiz Miner. Petrogr Mitt* 78, 243–255.
- 928 Zhou, H., Hoernle, K., Geldmacher, J., Hauff, F., Homrighausen, S., Garbe-Schönberg, D., Jung, S.,  
929 2020. Geochemistry of Etendeka magmatism: Spatial heterogeneity in the Tristan-Gough  
930 plume head. *Earth Planet. Sci. Lett.* 535, 116123. <https://doi.org/10.1016/j.epsl.2020.116123>
- 931
- 932

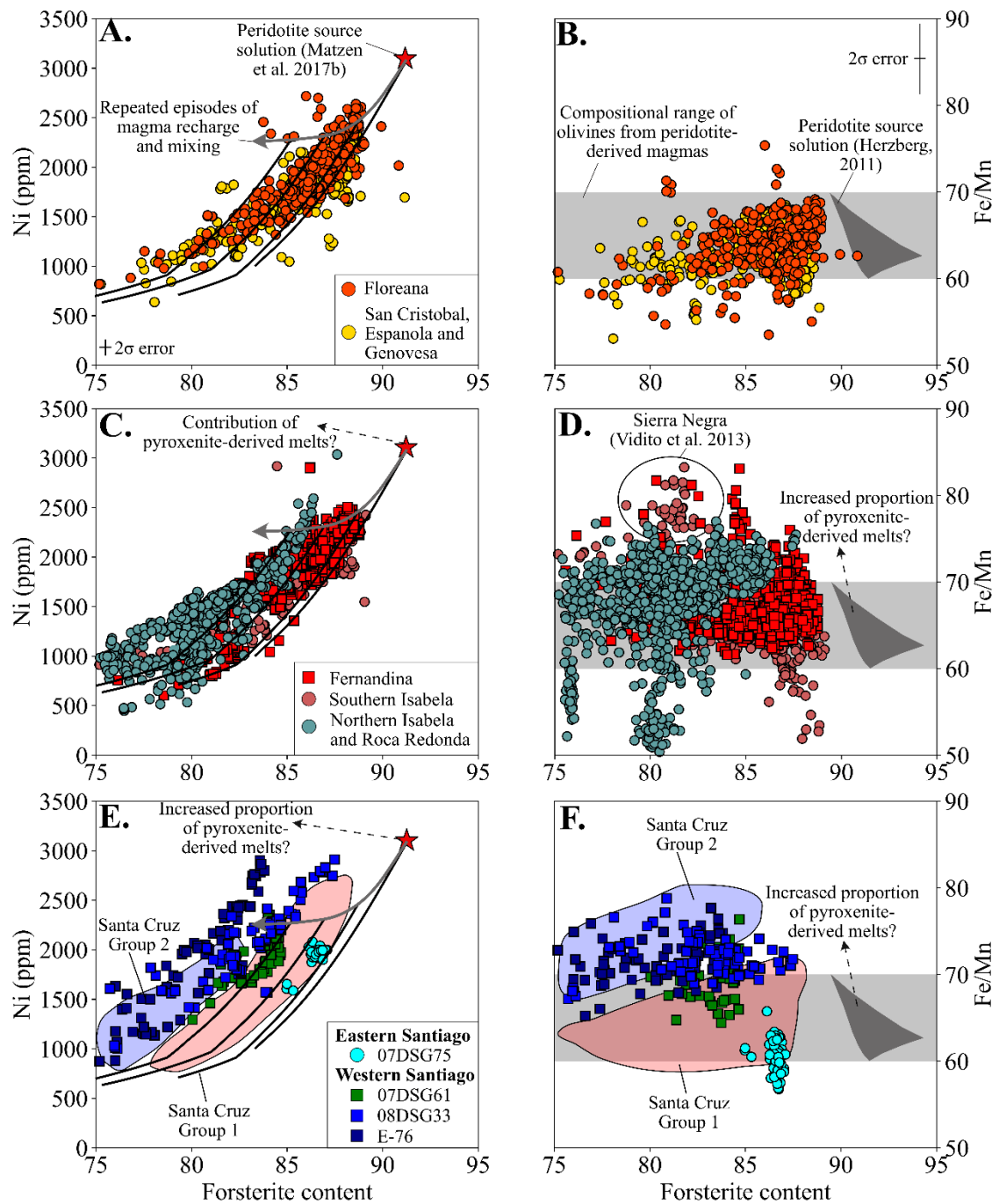
933 **FIGURE CAPTIONS**

---





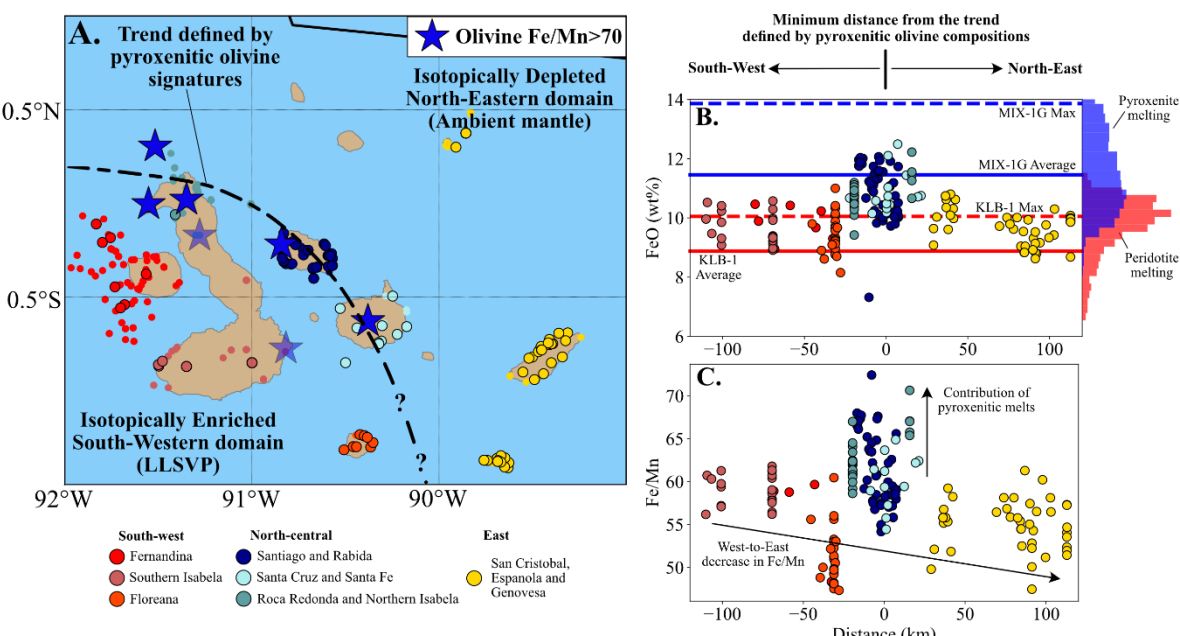
942 **Figure 2** – Variation in the composition of basalts erupted across the Galápagos Archipelago. **A.**  
943 Spatial variations in the  $^{143}\text{Nd}/^{144}\text{Nd}$  composition of the Galápagos basalts. Less radiogenic, and thus  
944 more enriched, Nd isotope signatures are observed in the south-western Galápagos. The enriched  
945 isotopic signature of Pinta is likely related to the transfer of compositionally enriched melts to the  
946 nearby Galápagos Spreading Centre (Gleeson and Gibson, 2021). **B.** Variations in the  $\text{FeO}_t$  content of  
947 high-MgO basalts erupted in the Galápagos (basalts with MgO contents above 8 wt% are shown).  
948 Notably, areas with the highest  $\text{FeO}_t$  contents are found in the north and central Galápagos, on the  
949 islands of Santiago, Santa Cruz, Roca Redonda, and on the northern margins of Isabela. **C.** Contours  
950 of lithospheric thickness (taken from Gibson and Geist 2010) that reveal the thickness of the  
951 lithosphere decreases eastwards in the Galápagos Archipelago. Data from Allan and Simkin, 2000;  
952 Bow and Geist, 1992; Geist et al., 2002, 2006, 2005; Gibson et al., 2012; Gibson and Geist, 2010;  
953 Harpp et al., 2003; Harpp and Weis, 2020; Kurz and Geist, 1999; McBirney and Williams, 1969;  
954 Naumann et al., 2002; Saal et al., 2007; Standish et al., 1998; Swanson et al., 1974; Teasdale et al.,  
955 2005; and White et al., 1993.



956

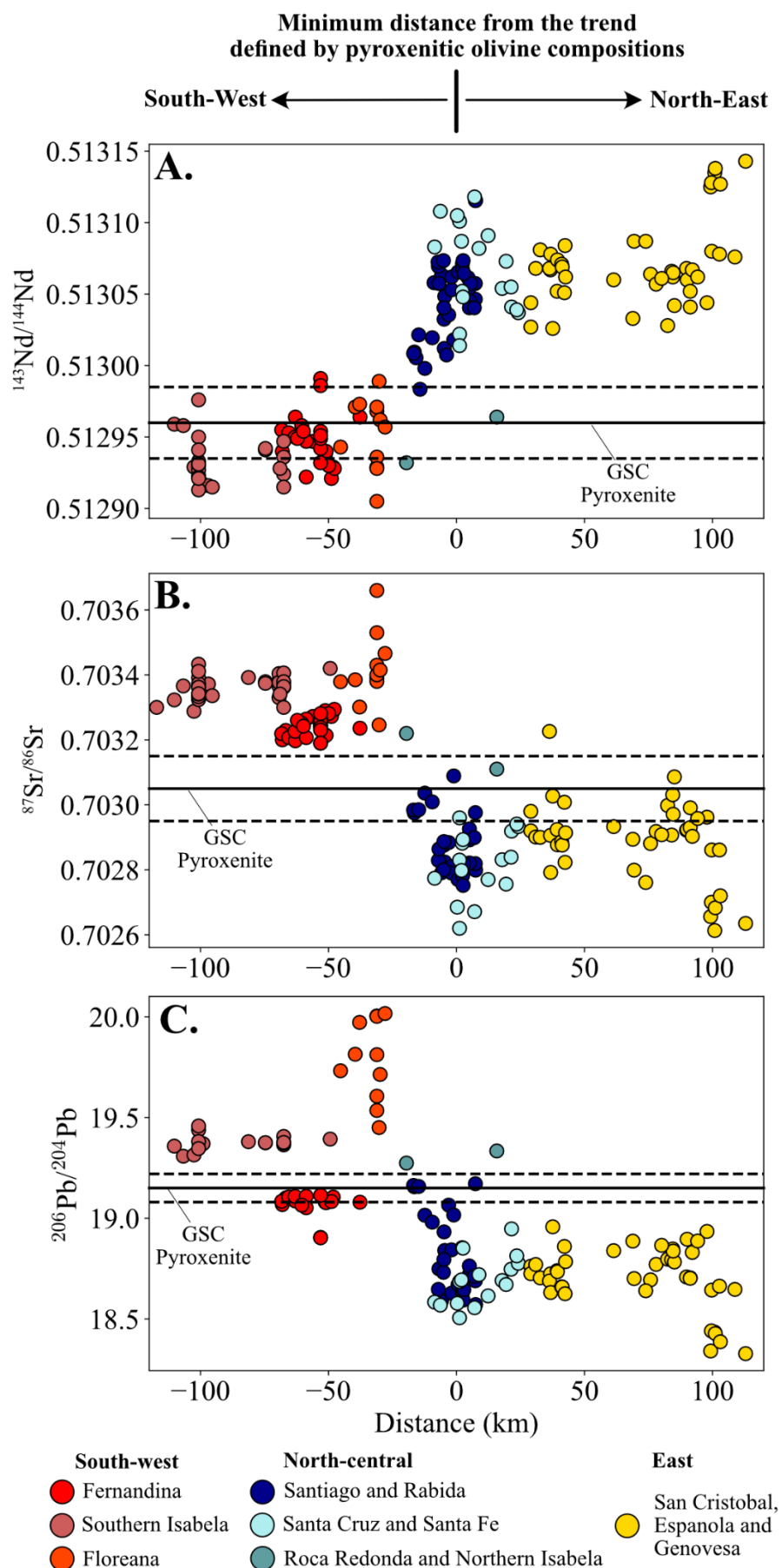
957 **Figure 3** – Composition of olivines from the eastern and southern Galápagos (**A, B**), western  
 958 Galápagos (**C, D**), and central Galápagos (**E, F**). **A.** Ni contents of olivines from islands in the  
 959 eastern Galápagos (Genovesa, Espanola, and San Cristobal) and Floreana in the southern Galápagos  
 960 are consistent with the compositions predicted to form from melts of a peridotite source. Data from  
 961 the western Galápagos (panels **C** and **D**) is typically consistent with the presence of a peridotitic

962 source. The Ni and Fe/Mn contents of olivines from northern Isabela and Roca Redonda, however,  
 963 are difficult to explain without invoking the presence of a lithologically distinct source component.  
 964 Olivine data from the central Galápagos (**E.** and **F.**) is more complex, the composition of olivines in  
 965 tholeiitic basalts from Santiago and Group 1 olivines from Santa Cruz are consistent with a peridotitic  
 966 source. Group 2 olivines from Santa Cruz and olivines in mildly alkaline basalts from Santiago,  
 967 however, require the presence of a lithologically distinct component in their mantle source.  
 968 Fractional crystallisation paths in **A.**, **C.**, and **E.** are taken from Gleeson and Gibson (2019). The range  
 969 of olivine Fe/Mn contents that are consistent with derivation from a peridotite source is taken from  
 970 (Herzberg, 2011). Peridotite source component taken from Matzen et al. (2017b) and Herzberg  
 971 (2011). Data from this study, Vidito et al. (2013), and Gleeson and Gibson (2019).



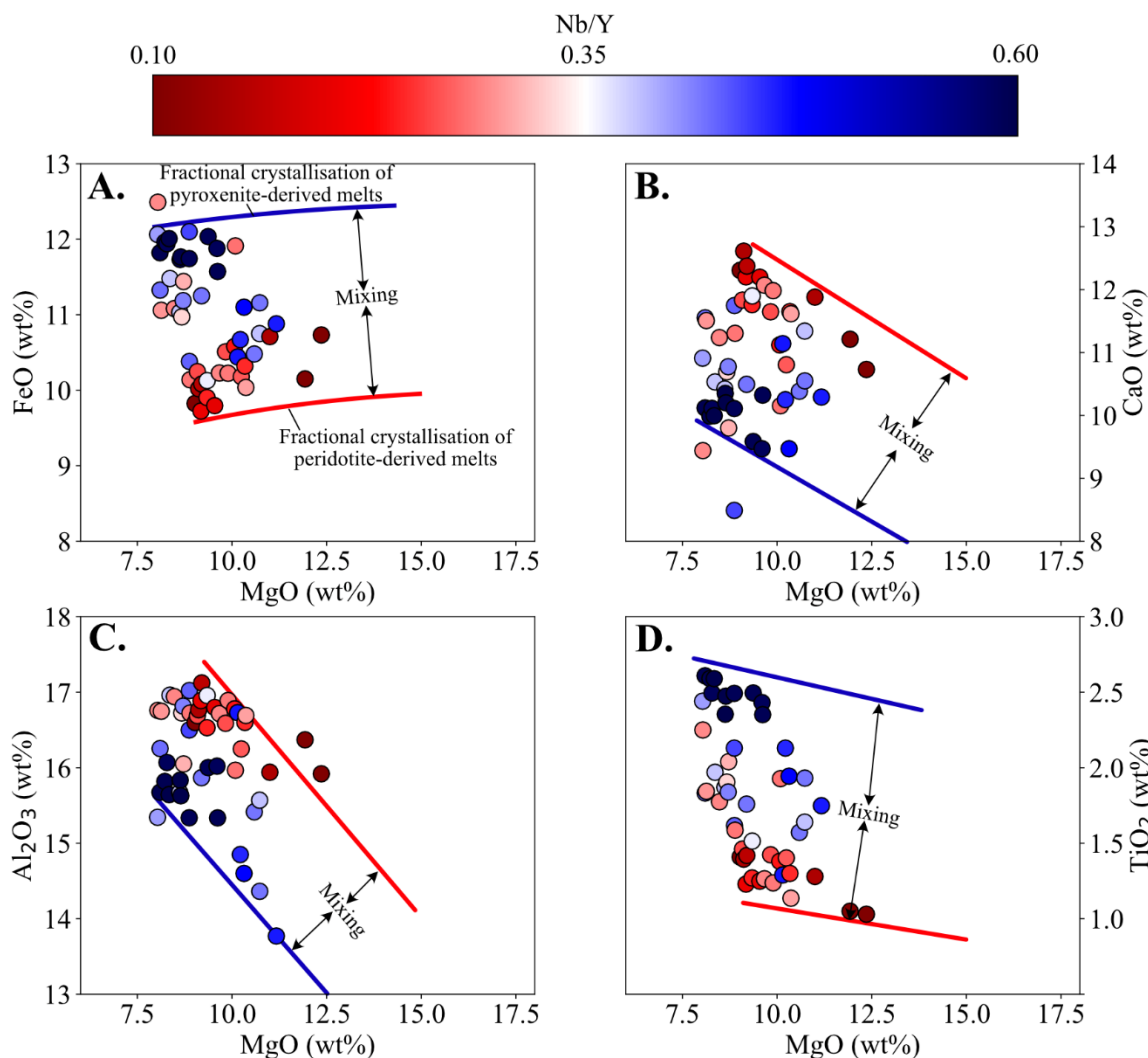
972  
 973 **Figure 4 – Major element systematics of the Galápagos basalts. A.** Location of basalts considered in  
 974 this study, those with MgO contents above 8 wt% are displayed with a black outline. Samples with  
 975 olivine Fe/Mn>70 are highlighted by the blue stars. Samples from Sierra Negra and Darwin are  
 976 partially transparent as the olivines measured from these volcanoes are very evolved. The black line  
 977 represents the approximate trend through this region with ‘pyroxenitic’ olivine compositions. Basalts  
 978 are broadly sub-divided into 3 categories: south-western basalts (reds); north-central basalts (blues);

979 and eastern basalts (yellow). **B.** The FeO<sub>t</sub> contents of high-MgO basalts are compared to their  
980 minimum distance to the black line plotted in **A.** (i.e., the location of basalts with ‘pyroxenitic’ olivine  
981 compositions). We find that the FeO<sub>t</sub> content of basalts from the south-western Galápagos and the  
982 north-eastern Galápagos are relatively constant, typically between 9 and 10.5 wt%. Notably, these  
983 FeO<sub>t</sub> contents are consistent with those measured in experimental melts of the KLB-1 peridotite  
984 (Hirose and Kushiro, 1993; Takahashi et al., 1993) and THERMOCALC v3.4.7 calculations of melting  
985 the KLB-1 peridotite (red histogram). Basalts from the north-central Galápagos, which plot within  
986 ~25 km of the black line shown in **A.**, have higher FeO<sub>t</sub> contents, up to 12.8 wt%. Such high FeO<sub>t</sub>  
987 contents require the presence of lithological heterogeneity in the mantle source. The average and  
988 max FeO<sub>t</sub> content of melting experiments on the pyroxenitic lithology MIX-1g is shown for reference  
989 (Hirschmann et al., 2003; Kogiso et al., 2003), and the FeO<sub>t</sub> contents predicted for melting of the  
990 MIX-1g pyroxenite in THERMOCALC v3.4.7 is shown by the blue histogram. **C.** The Fe/Mn ratio of  
991 high-MgO basalts from across the Galápagos shows a general decrease from west to east. Notable  
992 exceptions to this trend are the basalts from the north-central Galápagos. Data from Allan and  
993 Simkin, 2000; Bow and Geist, 1992; Geist et al., 2002, 2006, 2005; Gibson et al., 2012; Gibson and  
994 Geist, 2010; Harpp et al., 2003; Harpp and Weis, 2020; Kurz and Geist, 1999; McBirney and Williams,  
995 1969; Naumann et al., 2002; Saal et al., 2007; Standish et al., 1998; Swanson et al., 1974; Teasdale et  
996 al., 2005; and White et al., 1993.



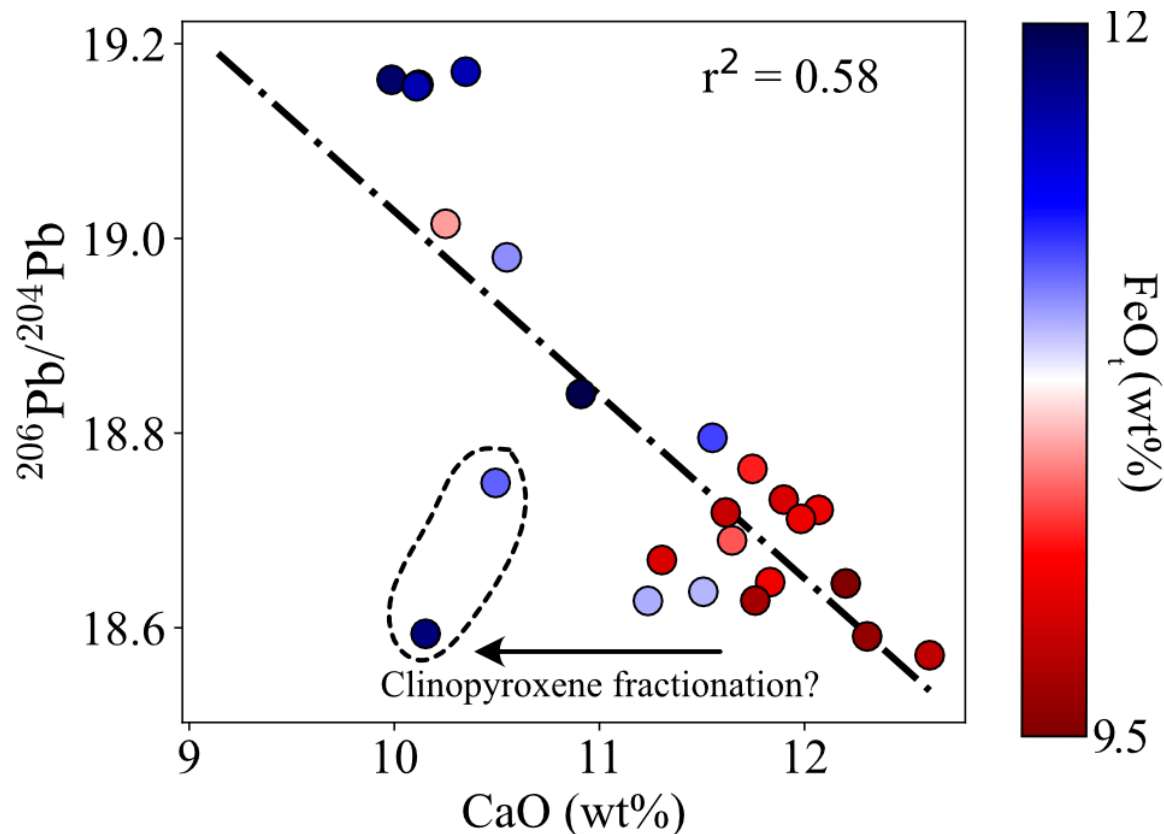
998 **Figure 5** – Radiogenic isotope composition of basalts from the Galápagos Archipelago. In all panels,  
999 the proposed isotopic composition of the pyroxenite component in the source region of the  
1000 Galápagos Spreading Centre basalts is shown by the black horizontal lines. These values are taken  
1001 from the work of Gleeson et al. (2020) and Gleeson and Gibson (2021) and the uncertainties in these  
1002 isotopic compositions were constrained using the python code presented in Gleeson and Gibson  
1003 (2021). Basalts from Roca Redonda, northern Isabela, and the most enriched basalts from Santiago,  
1004 have very similar isotopic systematics to this proposed end-member. Data from Allan and Simkin,  
1005 2000; Bow and Geist, 1992; Geist et al., 2002, 2006, 2005; Gibson et al., 2012; Gibson and Geist,  
1006 2010; Harpp et al., 2003; Harpp and Weis, 2020; Kurz and Geist, 1999; Mc Birney and Williams, 1969;  
1007 Naumann et al., 2002; Saal et al., 2007; Standish et al., 1998; Swanson et al., 1974; Teasdale et al.,  
1008 2005; and White et al., 1993.

1009



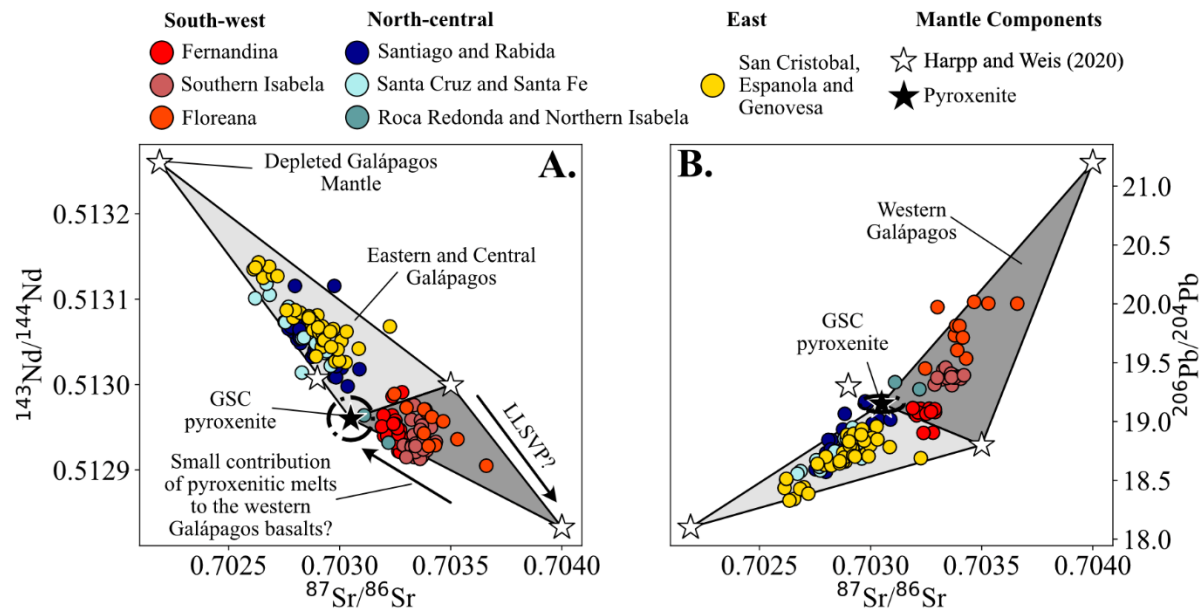
1010

1011 **Figure 6** – Major element systematics of basalts from Santiago, Santa Cruz, Rabida and Santa Fe with  
 1012 MgO contents >8 wt%. The major element systematics of the high-MgO basalts are related to their  
 1013 isotopic and trace element signatures (represented here by their Nb/Y ratio). Pyroxenite melts  
 1014 contain high FeO<sub>t</sub> and TiO<sub>2</sub>, but lower CaO and Al<sub>2</sub>O<sub>3</sub> contents than the peridotitic melts, consistent  
 1015 with experimental data (Lambert et al., 2013). Blue and red lines display the olivine fractionation  
 1016 curves, calculated by removing olivine whose composition is calculated using the olivine K<sub>d</sub> of  
 1017 Herzberg and O'Hara (2002), for hypothetical pyroxenite-derived and peridotite-derived melts,  
 1018 respectively. Data from Gibson et al., 2012; Gibson and Geist, 2010; Harpp and Weis, 2020; Mc Birney  
 1019 and Williams, 1969; Saal et al., 2007; and White et al., 1993.



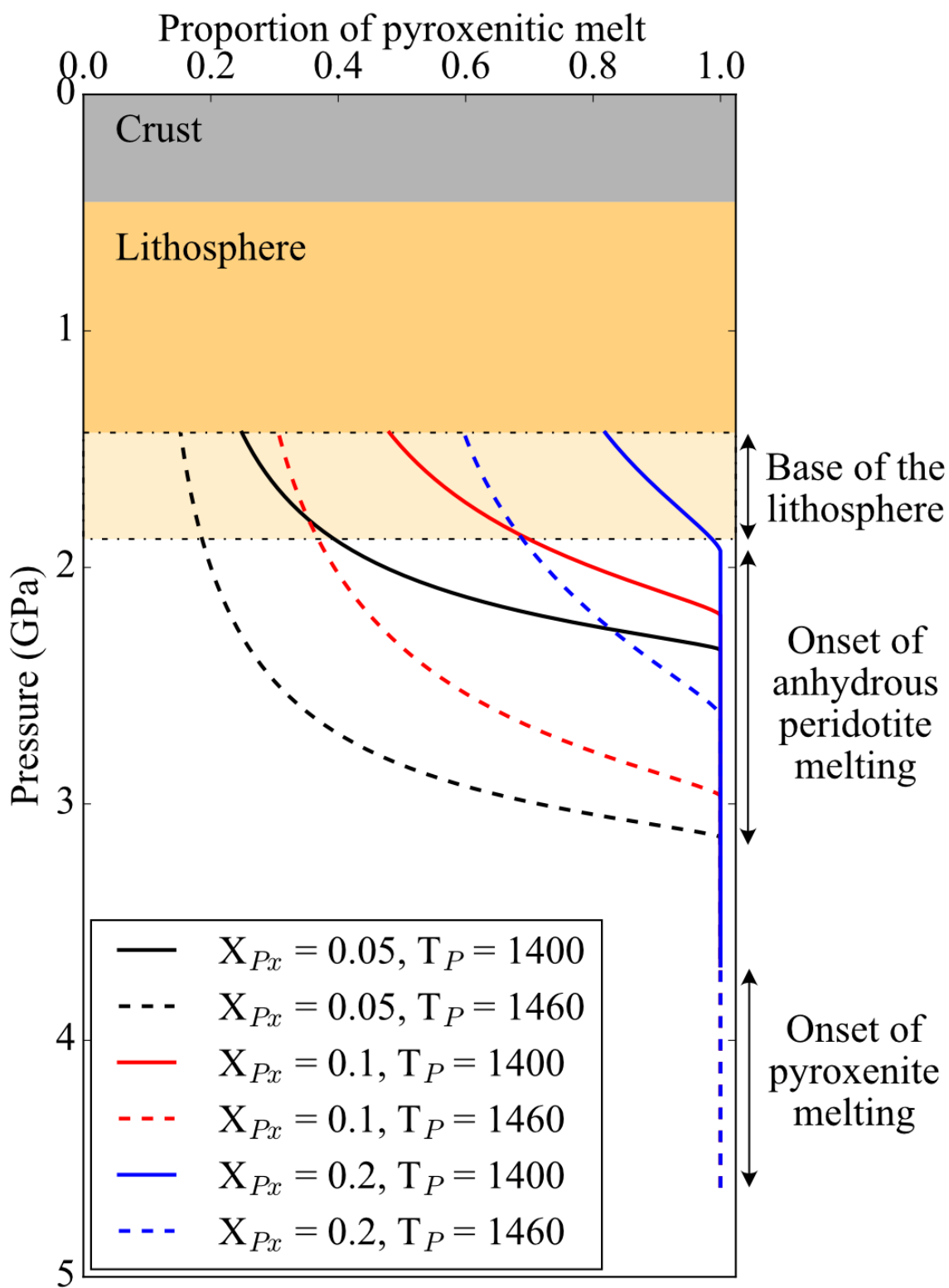
1020

1021 **Figure 7** – Correlation between the major element systematics of the high-MgO Santiago basalts  
1022 ( $\text{MgO} > 8 \text{ wt\%}$ ) and radiogenic isotopes. Strong correlations that are significant at the 99%  
1023 confidence level are observed between  $\text{CaO}$  or  $\text{FeO}_t$  and the radiogenic isotope ratios considered in  
1024 this study ( $^{87}\text{Sr}/^{86}\text{Sr}$ ,  $^{143}\text{Nd}/^{144}\text{Nd}$ ,  $^{206}\text{Pb}/^{204}\text{Pb}$ ) and confirm the relationship between isotopic  
1025 enrichment and pyroxenitic contribution in the central Galápagos. Two samples with low  $\text{CaO}$   
1026 contents and unradiogenic  $^{206}\text{Pb}/^{204}\text{Pb}$  signatures might result from unfiltered clinopyroxene  
1027 fractionation, but we expect the influence of plagioclase and clinopyroxene fractionation to be  
1028 minor in most Galápagos basalts considered here (see Supplementary Information). Data from  
1029 Gibson et al. (2012).



1031 **Figure 8 –** Isotopic composition of the Galápagos basalts compared to the proposed mantle end-  
 1032 members from Harpp and Weis (2020) and the proposed isotopic composition of the Galápagos  
 1033 pyroxenite component (determined using the models presented by Gleeson and Gibson (2021)).  
 1034 There is a clear divide between the isotopic composition of basalts from the south-western  
 1035 Galápagos and those from the central and eastern Galápagos. We suggest that the isotopic  
 1036 composition of basalts from the eastern and central Galápagos are controlled by mixing of melts  
 1037 from the DGM and the proposed pyroxenitic end-member (potentially with a minor contribution  
 1038 from LLSVP material). On the other hand, basalts from the south-western Galápagos are primarily  
 1039 sourced from LLSVP material, but small contributions of pyroxenitic material may influence their  
 1040 isotopic systematics.

1041



1042

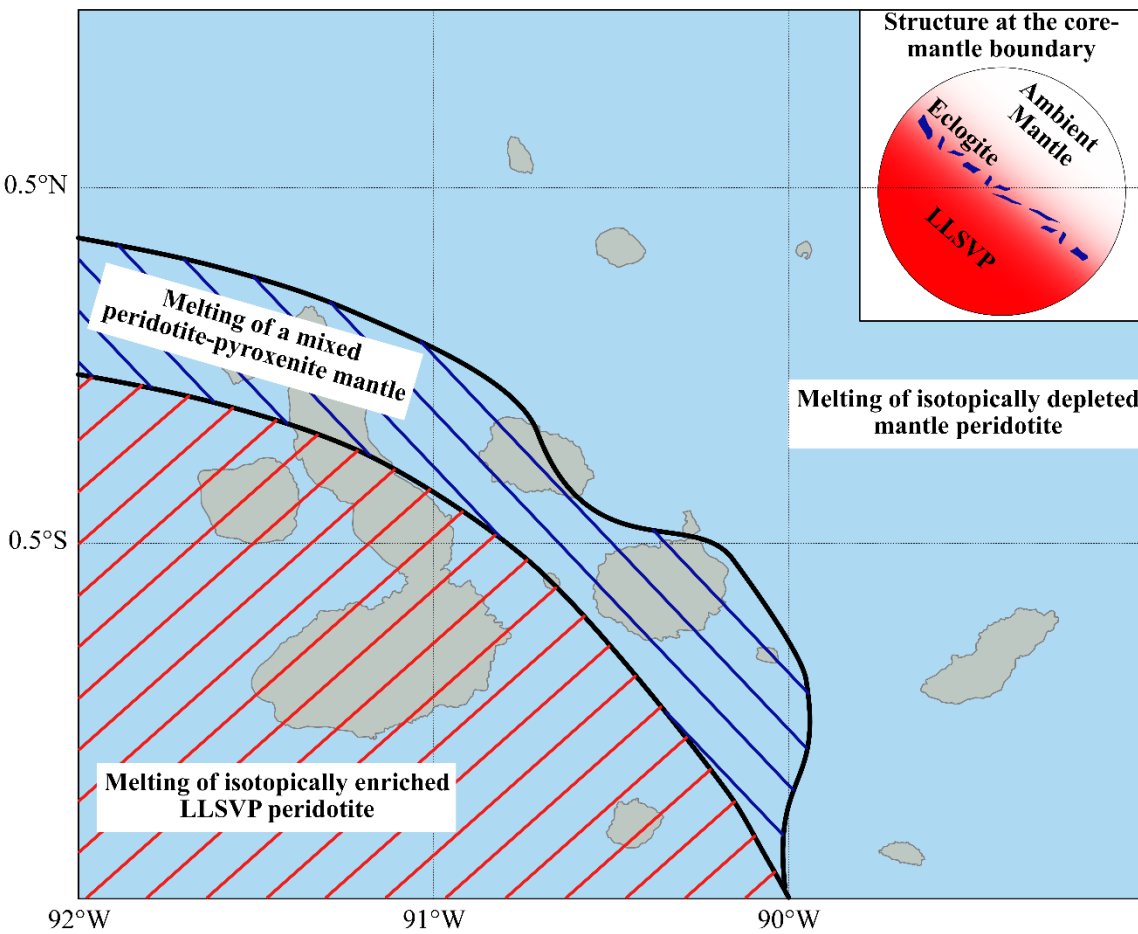
1043 **Figure 9** – Proportion of pyroxenitic melt predicted from melting of a two-component mantle.

1044 Calculations were performed in the pymelt module (Matthews et al., 2020) over a range of initial

1045 parameters, including the proportion of pyroxenite (formed as the reaction product of melts of

1046 subducted oceanic crust and peridotite) in the source ( $X_{Px}$ ), the mantle potential temperature ( $T_p$ ),  
1047 and the pressure at the base of the lithosphere.

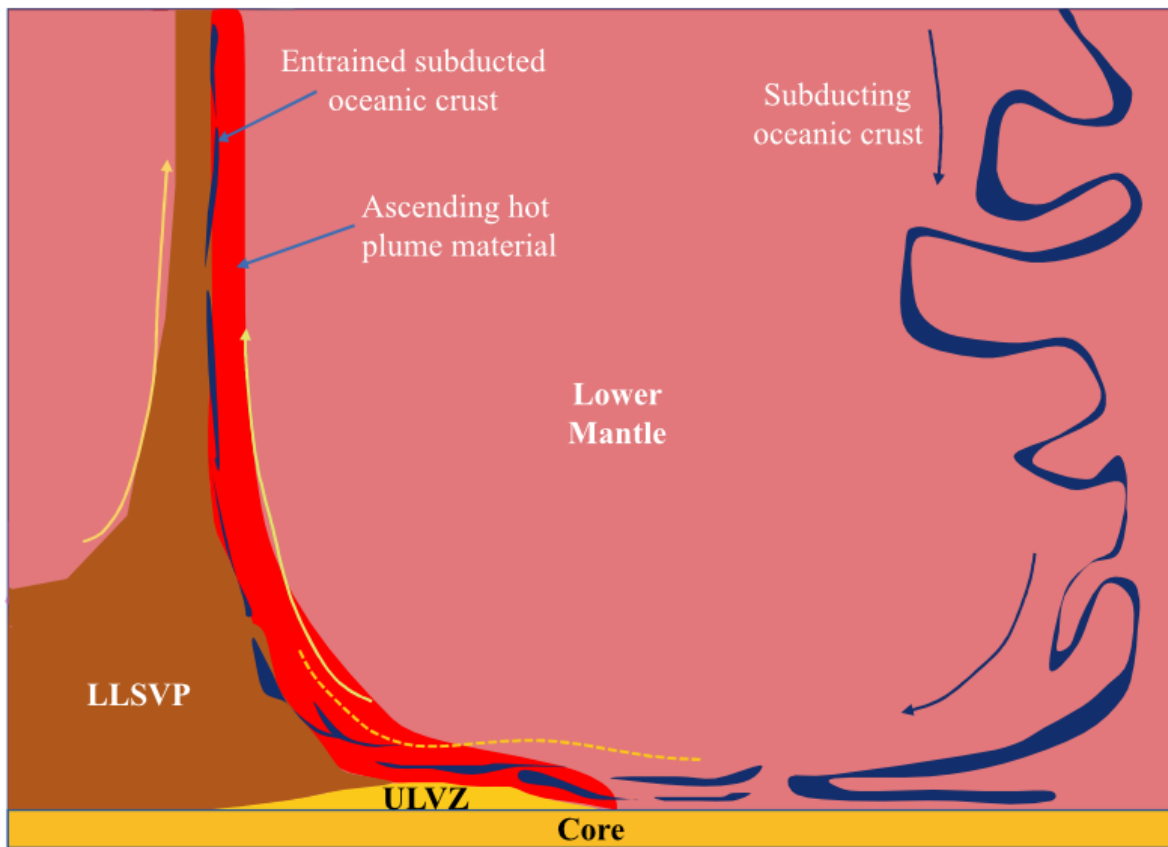
1048



1049

1050 **Figure 10 –** Distribution of peridotite and pyroxenite in the mantle source region of the Galápagos  
1051 basalts. The isotopically enriched mantle beneath the south-western Galápagos displays no evidence  
1052 for lithological heterogeneity and is thus interpreted to be peridotitic. As a result, there is no  
1053 evidence in the Galápagos to suggest that the Pacific LLSVP represents a pile of subducted oceanic  
1054 crust. In the north-central Galápagos the chemistry of the erupted basaltic lavas is controlled by  
1055 mixing of melts from a pyroxenitic mantle source, formed through the reaction of melts from  
1056 subducted oceanic crust (eclogite) with surrounding mantle peridotite, and upwelling mantle

1057 peridotite. In the eastern Galápagos, the depleted nature of the basalts indicates that the mantle  
1058 source is dominated by isotopically depleted peridotitic mantle.



1059  
1060 **Figure 11** – Schematic of the possible structure of the Pacific LLSVP margin at the base of the  
1061 Galápagos mantle plume. Subducted oceanic lithosphere is present near the margin of the LLSVP  
1062 leading to the steep LLSVP margin and the spatial distribution of lithological heterogeneity in the  
1063 Galápagos mantle plume. The Galápagos plume has a complex asymmetric structure, with peridotitic  
1064 mantle rising on the north-eastern side of the plume and enriched LLSVP material rising on the  
1065 south-western side. The LLSVP is likely formed from primordial material. Figure adapted from  
1066 Stevenson (2019).